Molecular relaxation of sucrose in aqueous solution: How a nanosecond molecular dynamics simulation helps to reconcile NMR data

ARTICLE *in* THE JOURNAL OF PHYSICAL CHEMISTRY B · SEPTEMBER 1995

Impact Factor: 3.3 · DOI: 10.1021/j100036a005

3 AUTHORS, INCLUDING:

Søren Balling Engelsen
University of Copenhagen
259 PUBLICATIONS **5,875** CITATIONS
SEE PROFILE

Serge Perez
French National Centre for Scientific Researc…
296 PUBLICATIONS **8,317** CITATIONS
SEE PROFILE

Molecular Relaxation of Sucrose in Aqueous Solution: How a Nanosecond Molecular Dynamics Simulation Helps To Reconcile NMR Data

Søren Balling Engelsen,[†] Catherine Hervé du Penhoat,[‡] and Serge Pérez*,[†]

Ingénierie Moléculaire, Institut National de la Recherche Agronomique, BP1627, 44316 Nantes, France, and Laboratoire de Chimie de l'Ecole Normale Supérieure, 24 rue Lhomond, 75231 Paris, France

Received: February 14, 1995; In Final Form: June 27, 1995[⊗]

The dynamical conformational behavior of sucrose in water was assessed through the combined use of molecular dynamics simulations and high-resolution NMR spectroscopy. Molecular dynamics simulations were performed in vacuum and in aqueous solution for 1 and 1.2 ns, respectively. Carbon relaxation data were established at 62.9 and 100.6 MHz; three-bond heteronuclear coupling constants were also determined. Two sets of phase-sensitive NOESY spectra were acquired. The presence of explicit water molecules in the simulation induces significant changes in the molecular potential. An important percentage of the glycosidic conformational space is populated, exemplifying the inherent conformational flexibility of sucrose. Hydration is inducing some conformational shifts, both in the glycosidic space and in the conformational space of the five-membered ring. The sucrose molecule is found to be extensively hydrogen bonded to water molecules. All of the potential intramolecular hydrogen bonds are exchanged to surrounding water molecules; of particular interest is the observation of a 25% populated water bridging conformation: O2-g···Ow···O3-f. However, neither of the two crystallographic intramolecular hydrogen bonds (O2-g···HO-1f and O5-g···HO-6f) persists durably in aqueous solution. A strong damping effect on high frequency motions is observed, but root-mean-square fluctuations are larger than those of the vacuum simulations. The softening of the molecular potential allows the crystal conformation of the sucrosyl raffinose to appear in a highly populated area of the conformational space. The radius of gyration, overall molecular tumbling time, and self diffusion coefficient of the sucrose in aqueous solution were established from the molecular dynamics simulations; they compare extremely well with the corresponding experimental values. Equally satisfactory is the good agreement obtained with the glycosidic heteronuclear coupling constant. The molecular dynamics simulation shows that the high-frequency oscillations of sucrose are severely damped by the presence of explicit water and that internal motions occur on the same time scale as the overall tumbling. For such a motional regime the second term in the model-free spectral densities cannot be ignored. Theoretical carbon longitudinal relaxation were fitted to experimental ones with the molecular dynamics model by adjusting the correlation times for internal motions. This model is very different from that previously proposed for sucrose in which internal motions are considered to be extremely rapid. The motional model was shown to be very satisfactory for calculating the NOESY volumes. Thus, the MD simulations were able to distinguish between two otherwise equally good motional models based on NMR relaxation data. The selected model would appear to be a fairly universal motional model for small carbohydrate molecules consistent with both proton and carbon relaxation data.

Introduction

Sucrose has been a leading world commodity for centuries. Since the beginnings of organic chemistry, it has always been considered a prototype molecule for establishing and refining general methods for structural elucidation. Sucrose (β-D-fructofuranosyl-α-D-glucopyranoside abbreviated as β-D-Fru*f*-(2−1)-α-D-Glc*p*) is a nonreducing disaccharide; its molecular conformation in anhydrous single crystals has been established from neutron and X-ray diffraction studies,[1−3] showing an almost spherical molecule stabilized by two intramolecular hydrogen bonds (O-1f−H···O-2g and O-6f−H···O-5g). Despite several investigations, the conformational behavior of sucrose in solution is still a matter of debate. In one of the first combined modeling and NMR studies,[4] sucrose was described as being nearly spherical, similar to its shape in crystalline sucrose and quite rigid. It was postulated that this preferred conformation was largely independent of the solvent used. Its inability to adjust to the exo-anomeric effect was explained by steric effects, and it was suggested that dilute aqueous sucrose has one intramolecular hydrogen bond. In an NMR investigation of sucrose in DMSO, Christofides and Davies[5,6] proposed the existence of two competing intramolecular hydrogen bonds (O-2g···O-1f, and O-2g···O-3f). However, it has been concluded that there is no evidence for persistent intramolecular hydrogen bonds based on the temperature coefficients of the NMR data for the hydroxyl protons of sucrose in a mixture of water and acetone.[7] Another joint NOE and molecular modeling study indicated that sucrose in aqueous solution is flexible and argued against the importance of the intramolecular hydrogen bond between O-2g and O-1f, with respect to the molecular conformation.[8] The results provided by other numerous experimental studies[9−18] do not provide a unified picture of the conformational behavior of sucrose in solution.

Sucrose has been extensively studied by molecular modeling methods. Tran and Brady[19,20] used the CHARMm[21] program and a potential function for carbohydrates[22] to investigate the sucrose energy surface through molecular statics and dynamics simulations. Subsequent conformational studies were conducted

† Institut National de la Recherche Agronomique.
‡ Laboratoire de Chimie de l'Ecole Normale Supérieure.
* Author for correspondence.
⊗ Abstract published in *Advance ACS Abstracts*, August 15, 1995.

0022-3654/95/2099-13334$09.00/0

using different versions of MM3[23,24] and slightly different protocols.[25-28] Most recently, the potential energy hypersurface of sucrose has been examined by molecular mechanics calculations (MM3) interfaced with two different algorithms for conformational searching.[28] From these conformational studies, which also took into account the flexibility of the glucopyranose and the fructopyranose rings, a consistent structural model is emerging for sucrose that indicates that it can display a variety of conformations. While all the previous theoretical works were conducted with the absence of explicit solvent, in particular water molecules, preliminary investigations[26] suggested that the conformational equilibrium of sucrose would be dependent on the nature of the solvent. With the availability of modern simulation methods, molecular mechanics simulations of carbohydrates in aqueous solution can be performed.[29-31] Obvious questions to be answered are the following: (1) What is the extent of intramolecular hydrogen bonding[32] and flexibility of sucrose in aqueous solution? (2) How does the aqueous solvation of sucrose influence the conformation about the glycosidic linkages and about the primary hydroxyl groups? (3) How do the theoretical structures compare to experimental ones as defined by homo- and heteronuclear NMR relaxation?

As molecular modeling methods have improved, it has become clear that carbohydrates are flexible molecules. Efforts have been made to account for the occurrence of such internal motions on the simulations of observed properties such as those derived from chiroptical and NMR measurements. One of the major difficulties in modeling relaxation data is evaluating the relative rates of molecular tumbling and internal motions. To this end, model-free spectral densities[33] have been used in several instances.[34-36] In several carbon relaxation studies of sucrose,[13,37,38] internal motion has been considered to be extremely rapid and the second term in these spectral density expressions has been ignored. This latter motional model, which has been widely adopted in the description of carbohydrates[39,40] was also used to simulate the magnetic field dependence of two homonuclear cross-relaxation rates of aqueous sucrose.[16] However, recent studies based on the fitting of the theoretical relaxation rates and NOESY volumes to experimental data have suggested that the second term in the model-free spectral densities cannot be ignored in the case of low molecular weight carbohydrates.[41,42]

A major goal of the present work was to examine the effect of solvation upon sucrose conformational behavior and to investigate the nature of its hydration. To this end, molecular dynamics simulations that explicitly include aqueous solvent molecules have been performed for a duration of 1.2 ns. Another major goal was to obtain a motional model that could reproduce the large experimental data base (^{1}H and ^{13}C relaxation parameters) that has been established for aqueous sucrose. It was hoped that a clear picture of the internal dynamics would emerge from a theoretical evaluation of the amplitude of the internal motions sampled from MD trajectories.

Methods

Nomenclature. A schematic representation of the nonreducing disaccharide sucrose (β-D-fructofuranose-(2→1)-α-D-glucopyranoside) along with the numbering and labeling of the heavy atoms is shown in Figure 1. Sucrose contains two neighboring anomeric centers C-1g and C-2f and exhibits an overlapping exo-anomeric effect due to the sequence C-5g−O-5g−C-1g−O-1g−C-2f−O-5f−C-5f. The sign of the torsion angles is defined in agreement with the IUPAC-IUB Commission of Biochemical Nomenclature.[43] The conformation about the glycosidic linkage bonds is described by the following

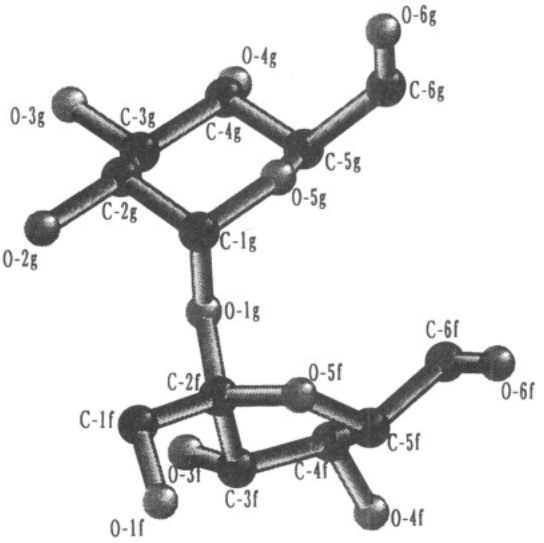

Figure 1. Schematic representation of sucrose inclusive numbering and labeling of the heavy atoms.

torsion angles:

$$\Phi = \text{O-5g}-\text{C-1g}-\text{O-1g}-\text{C-2f}$$

$$\Psi = \text{C-1g}-\text{O-1g}-\text{C-2f}-\text{O-5f}$$

The orientations of the three hydroxymethyl groups are described by the torsional angles:

$$\omega_g = \text{O-5g}-\text{C-5g}-\text{C-6g}-\text{O-6g}$$

$$\omega_f = \text{O-5f}-\text{C-5f}-\text{C-6f}-\text{O-6f}$$

$$\chi_f = \text{O-5f}-\text{C-2f}-\text{C-1f}-\text{O-1f}$$

The orientations are also referred to as either gauche−gauche (GG), gauche−trans (GT), or trans−gauche (TG) depending on whether the values of the above torsion angles are closest to −60°, 60°, and 180°. Another parameter of interest is the magnitude of the valence angle at the glycosidic linkage C-1g−O-1g−C-2f.

The ring shape of the flexible five-membered furanose ring can be defined by two puckering parameters.[44,45] Their description involves an amplitude that measures the deviation from planarity and a phase angle that describes the type of distortion. Throughout this paper we use the Cremer−Pople convention[45] which uses the two parameters q_2 and ϕ_2 to describe the ring conformation of the furanose moiety and which can easily be related to one of the 20 different twist (T) and envelope (E) shapes that can be adopted by a five-membered ring.

NMR Spectroscopy. ^{1}H (250.14 MHz) and ^{13}C NMR (62.9 and 100.6 MHz) spectra were recorded with Bruker instruments operating in the Fourier transform mode at 296 K unless stated otherwise. Chemical shifts (assigned from 2D spectra) and vicinal coupling constants, $^3J_{H,H}$, were extracted from a spectrum with a digital resolution of 0.12 Hz/point. Both double irradiation techniques and simulation of the 1D spectrum using the Bruker package PANIC were required to obtain the coupling constants and chemical shifts of protons whose signals were in overlapping regions.

^{13}C T_1 measurements were acquired with the inversion−recovery sequence (180−τ−90−FID) and relaxation times were calculated with the Bruker T_1 routine. Two sets of phase-sensitive NOESY spectra[46] were acquired with mixing times of 0 and 1 s. A 20 ms variable delay was introduced at the beginning of the mixing time in order to suppress J-peak

transfer.[47] The recycle time was set to 5 times the longest T_1 in order to obtain a symmetrical normalized NOESY volume matrix. The diagonal and cross peak intensities were evaluated from the summed ω_1 subspectra contributing to a specific signal. The standard (average) deviations were calculated for the cross-peak volumes, $a_{k,l}$ (diagonal volumes, $a_{k,k}$). Integration of noise in these spectra gave ±0.005 units of normalized intensity with respect to the diagonal volume (τ_m = 0 s) for typical peak widths.

Computational Methods. The solution behavior of sucrose was investigated using the carbohydrate force field developed by Ha et al.,[22] referred to as the HGFB force field, and recently applied to maltose in solution by Brady and Schmidt.[31] The force field which was implemented in the general molecular mechanics CHARMm program[21] is a typical standard type of molecular mechanics force field. It has been developed as a "true vacuum type" potential, and it is currently regarded as one of the best potentials for reproducing solution behavior of carbohydrates in the presence of water. The force field has no explicit hydrogen-bonding potential, i.e., hydrogen bonds are modeled as a combination of attractive van der Waals and Coulombic forces. The water molecules of the solvent were modeled using the TIP3P potential energy function.[48]

Molecular Statics (MS). Grid Search. The potential energy surface of sucrose was computed from 54 individual relaxed potential energy maps in vacuum. The starting conformations of the pyranosyl group were in all cases taken as $^4C_1$ and the corresponding starting conformers for the furanosyl moiety were taken as the crystallographic northern conformation. For all 27 possible combinations of orientations (GG/GT/TG) of ω_g, ω_f, and χ_f a clockwise (c) and a reverse clockwise (r) orientation of the secondary hydroxyl groups on the glucopyranosyl ring were considered, so as to best form a partial crown of weak intramolecular hydrogen bonds. Each of these conformations was fully optimized and used as a starting point for calculating a relaxed map. The relaxed maps were computed using rigid rotation followed by harmonic constraint minimization in 10° increments for Φ and Ψ spanning Φ in the range between 0 and 180° and the whole angular range of Ψ. Convergence was accepted when the root-mean-square (rms) gradient was less than 0.001 kcal/(mol Å^2) in the iterative conjugate gradient minimization algorithm. No cutoff of long-range nonbonded interactions was introduced in the energy calculations. For each point on this grid, the optimized coordinates and the corresponding energy were stored for further calculations. This approach resulted in 36 936 possible conformations of which 24 725 were accepted for further calculations on the basis of relative energy (≤20 kcal/mol) and nonredundant values of χ and χ' which were not constrained in the relaxed map calculations. A general adiabatic Φ,Ψ map was constructed by using the lowest energy values for the 54 relaxed maps. Isoenergy contour lines were plotted within an 8 kcal/mol range above the global minimum.

Molecular Dynamics (MD). An ensemble of five microcanonical sucrose trajectories in an explicit water phase were recorded, resulting in a total simulation time of 1.2 ns. For comparative purposes a single 1 ns sucrose trajectory was recorded in vacuum. The details of the six trajectories are listed in Table 1.

In the simulations reported here, Newton's equations of motion were integrated for each atom using the two-step velocity Verlet algorithm[49] implemented in the general molecular mechanics program CHARMm.[21] All hydrogen atoms were explicitly included although bond lengths involving hydrogen were kept fixed throughout the simulations using the constraint algorithm SHAKE.[50] The step size in the integration algorithm was 1 fs in all cases allowed by the use of the SHAKE algorithm which removes the fastest atomic motions, namely, the O−H stretchings ($\sigma \approx 3600$ cm^{-1}):

$$\omega_{min} = 1/\nu_{max} = 1/(\sigma_{max}c) = 1/(3600\ \text{cm}^{-1} \times 3 \times 10^{10}\ \text{cm/s}) \approx 10\ \text{fs} \quad (1)$$

When these fastest atomic motions are removed, the step size of 1 fs in the integration algorithm is far from the theoretical stability limit ($\Delta t = \omega_{min}/\pi$) and well below the practical stability limit of the Verlet algorithm.[50]

The explicit water phase was mimicked in the form of 512 TIP3P water molecules captured in a cubic box using minimum image periodic boundary conditions. Interactions between atoms more than 12 Å apart were truncated and switching functions were used to smoothly turn off long-range interactions between 10 and 11 Å. To avoid artificially splitting dipoles at the cutoff border, the switching functions were applied on a group-by-group basis, with the groups corresponding to complete water molecules and to electrostatically neutral groups in the solute.[21,29,51]

The initial coordinates of the solute were taken as respectively the X-ray structure,[1] here labeled **SX**, and the four minimum structures taken from the potential energy surface of sucrose[28] in the MM3 potential[23,24] labeled respectively **S1**, **S2**, **S3**, and **S4** (see Table 2). The latter choice was an attempt to avoid a biased choice in the HGFB force field which has a tendency to overemphasize intramolecular hydrogen bonds in vacuum[19] and to begin with pseudo preequilibrated structures. The vacuum trajectory was started from the **SX** conformation.

The initial coordinates for the systems were prepared by superimposing the starting coordinates of the solute upon the coordinates of a well equilibrated box of pure TIP3P water. Those water molecules whose van der Waals radii overlapped with any of the atoms in the sucrose solute were deleted from the system, leaving approximately 490 water molecules in the primary box (see Table 1). After the "solvation", the system was energy minimized with 50 steepest descent iterations with the original box size in order to relax steric conflicts which might have been created in the generation of the box and in order to relax the MM3/X-ray structures in the new potential. Then the cubic box size was adjusted slightly to give the experimental density[52] for the actual concentration (see Table 1). Initial velocities for all atoms were assigned from a Boltzmann distribution at 300 K, the same temperature at which the box of pure water was equilibrated. The systems were equilibrated respectively for 10 ps (**TS1**, **TS2**, **TS3**, **TS4**) and 20 ps (**TSX**) to relax any artificial starting conditions produced

TABLE 1: Characteristics of the Recorded Trajectories

trajectory	TSV	TSX	TS1	TS2	TS3	TS4
initial conformation	SX	SX	S1	S2	S3	S4
no. of water molecules	0	489	489	491	488	490
periodic box size (Å)		24.657	24.657	24.689	24.640	24.673
concn (% w/w)		3.74	3.74	3.73	3.75	3.74
density (kg/L)		1.013	1.013	1.013	1.013	1.013
ref temp (K)	300	300	300	300	300	300
total sampled time (ps)	1000	500	230	150	170	150
equilibration period (ps)	100	20	10	10	10	10
coordinate sampling (ps)	0.02	0.02	0.02	0.02	0.02	0.02

TABLE 2: Geometries of the Minimum Structures in MM3[28] (Minima S2, S3, and S4 Were Found To Be Respectively 0.26, 2.32, and 3.17 kcal/mol above the Global Minimum S1; Distances in angstroms and Angles in degrees)

conformation	X-ray	S1	S2	S3	S4
Φ	107.8	109.9	70.6	75.5	92.7
Ψ	−44.8	−59.9	−89.1	166.4	57.0
θ	114.3	117.5	119.4	122.0	120.6
ω_g	−56.4	70.5	70.1	66.2	68.8
ω_f	−69.6	71.0	68.8	−65.8	71.4
χ_f	171.4	−175.2	−173.9	−168.7	−171.9
q_2	0.353	0.425	0.425	0.440	0.399
ϕ_2	265.2	272.1	273.2	254.2	281.2
r_g	3.17	3.21	3.15	3.17	3.22
HO-2g···O-5f	4.695	4.222	4.486	3.535	4.630
O-5g···HO-3f	4.351	5.056	4.999	3.398	3.229
O-5g···HO-6f	**1.894**	4.921	4.895	5.958	6.426
O-5g···HO-1f	4.311	5.660	4.726	**2.126**	5.500
O-2g···HO-1f	**1.851**	3.345	4.887	5.340	5.897
HO-2g···O-1f	3.053	**2.231**	3.820	5.290	6.091
O-2g···HO-3f	4.701	3.916	3.751	5.054	5.604
HO-2g···O-3f	5.546	3.511	2.975	4.242	6.295
O-1g···HO-6f	2.963	5.484	5.128	3.883	5.706
O-2g···HO-6f	5.188	7.891	7.485	3.248	5.619
HO-2g···O-6f	6.520	7.018	6.862	**1.974**	6.040
HO-6g···O-6f	3.614	4.802	3.886	8.326	7.266
O-6g···HO-6f	3.421	4.175	3.008	8.122	8.709

by the solvation procedure, with occasional scaling of the atomic velocities when the average temperature deviated from the desired temperature of 300 K by more than an acceptable tolerance of ±3 K. Following the equilibration period, the integration was continued without further interference. Energy was well conserved in the simulations, with the average rms fluctuations in the Hamiltonian divided by those of the kinetic energy being less than 0.0035 kcal/mol when collected in 4 ps intervals of the production dynamics trajectories. The rms fluctuations in the temperature were about 6 °C.

The sucrose trajectory in vacuum was thermalized by increasing the temperature by 15 K in 1 ps intervals by a velocity reassignment procedure until the desired value of 300 K was obtained, resulting in a heating period of 20 ps. The heating period was followed by an equilibration period of 80 ps where atomic velocities were scaled if the temperature deviated from the desired value by more than ±3 K. Following the thermalization period the molecular system was allowed to evolve without further interference for subsequent 900 ps.

The ensemble simulation represented here required approximately 60 CPU days on a IBM RISC 6000 Model 340 computer. Approximately twice the CPU time was spent in total, including recording experiments with less-well-equilibrated systems.

Calculation of Diffusion Coefficients. The translational diffusion coefficient, D, is calculated using the Stokes−Einstein relationship by monitoring the mean-square displacement autocorrelation function for the solute center of mass, r:[30,53]

$$D(t) = \langle [r(t_0 + t) - r(t_0)]^2 \rangle / 6t \qquad (2)$$

Calculation of Coupling Constants. Coupling constants, $^3J_{H,H}$, for vicinal hydrogen atoms of a H−C−C−H segment were calculated using a Karplus type equation with the Haasnoot−Altona parametrization:[54]

$$^3J_{H,H} = P_1 \cos^2(\theta) + P_2 \cos(\theta) + P_3 + \sum \Delta\chi_i (P_4 + P_5 \cos^2(\xi_i \theta + P_6 |\Delta\chi_i|)) \qquad (3)$$

It accounts for J dependence on the dihedral angle (θ) of the H−C−C−H fragment, on the electronegativity of participating atoms[55] and on the orientation of the α and β substituents. The heteronuclear coupling constant $^3J_{H,C}$ across the glycosidic linkage was calculated by using the equation for the C−O−C−H segment proposed by Tvaroska et al.:[56]

$$^3J_{H,C} = 5.7 \cos^2(\Phi^H) - 0.6 \cos(\Phi^H) + 0.5 \qquad (4)$$

where

$$\Phi^H = (\text{H-1g−C-1g−O-1g−C-2f})$$

Rotamer distributions about primary hydroxyl groups were calculated numerically from the limiting values given by the Haasnoot−Altona equation[54,57] by solving the set of linear equations:

$$\begin{aligned} 0.9 \quad 10.7 \quad & 5.0 \times p_{GG} = J_{5,6R} \\ 2.8 \quad 3.1 \quad & 10.7 \times p_{GT} = J_{5,6S} \\ 1.0 \quad 1.0 \quad & 1.0 \times p_{TG} = 1.0 \end{aligned} \qquad (5)$$

where the p's are the fractional populations and J's are the coupling constants (hertz). For consistency we chose to recalculate all rotamer distributions using this set of equations. The results (Table 3) include negative populations arising from the inherent inaccuracies in the Haasnoot−Altona description and from the simplified model in which only idealized staggered conformations are considered.

Calculation of Relaxation Data and NOESY Volumes. The measurement of NMR relaxation parameters such as T_1, T_2, and NOE provides information on the atomic level concerning not only the magnitude of the internal motions but also on their time scale. In flexible carbohydrate systems, such as the ones investigated here, several different local conformations exist, but interconversions are rapid on the time scale of the NMR experiment wherefore average values are observed. In such cases, full quantitative analysis of NOE measurements requires realistic structural models (molecular dynamics simulations with solvent) to monitor the motional properties.

To account for internal motions in the treatment of relaxation data,[58,59] it is necessary to know the relative rates of overall tumbling, τ_c, and conformational exchange, τ_e. The flexibility can be accounted for by either $\langle r^{-3} \rangle$ or $\langle r^{-6} \rangle$ averaging depending on whether internal motions are considered to be rapid or slow with respect to molecular tumbling. This assumes that the overall and internal motions are not correlated, which is reasonable when the rates are separated by several orders of magnitude. If internal motions occur faster than the tumbling time of the molecule, the fluctuations in inter-hydrogen distances will arise essentially from internal motions. The so-called model-free approach proposed by Lipari and Szabo[33] may be applied to take into account the effects of such motions on the corresponding NOE data. If internal motions are slower than overall tumbling but fast with NOE buildup times, then the angular component of the dipolar interaction will be averaged by the tumbling, and ensemble average NOEs can be calculated from the ensemble average of the inverse sixth power of the inter-hydrogen distances. The intermediate case, in which internal motions occur on a time scale comparable to that of the overall tumbling, requires the full dipolar interaction, both angle and distance, to be evaluated from the molecular dynamics trajectory. Both the procedure used to average the internuclear distances obtained with molecular mechanics and the spectral density functions appropriate for calculation of cross-relaxation rates from internuclear distances require knowledge of these rates of motion. Investigations on different oligosaccharides

TABLE 3: Observed and Calculated ^3J Coupling Constants of Sucrose

^3J	exp[a]	MS[b]	TSV[c]	TSX[c]	TS1[c]	TS2[c]	TS3[c]	TS4[c]
				$^3J_{HH}$				
α-Glc*p*								
H-1g−H-2g	**3.8**	3.0	3.1	3.2	3.3	3.3	3.2	3.3
H-2g−H-3g	**10.0**	10.4	10.1	10.1	10.1	10.1	10.1	10.1
H-3g−H-4g	**9.1**	9.8	9.5	9.5	9.6	9.6	9.5	9.6
H-4g−H-5g	**9.8**	9.8	9.6	9.6	9.6	9.6	9.6	9.7
H-5g−H-6gS	**2.0**	10.6	10.2	4.8	10.2	7.3	9.2	3.7
H-5g−H-6gR	**5.0**	5.1	4.7	2.3	4.1	6.5	5.0	8.6
GG:GT:TG	65:47:−12[d]	9:1:90	0:0:100	77:0:23	1:1:98	0:40:60	0:14:86	0:84:16
Fru*f*								
H-3f−H-4f	**8.8**	8.8	6.0	4.5	2.9	4.9	2.7	7.1
H-4f−H-5f	**8.3**	7.9	5.8	4.8	3.2	5.8	3.9	8.1
H-5f−H-6fS	**7.1**	3.8	4.6	7.5	8.9	6.9	7.8	7.3
H-5f−H-6fR	**3.7**	1.4	2.2	5.6	5.1	6.7	3.6	4.4
GG:GT:TG	40:6:54[d]	97:0:3	81:1:18	13:23:64	0:15:85	0:44:56	32:1:67	33:9:58
				$^3J_{CH}$				
H1g−C-2f	**4.2**	5.4	5.3	4.1	3.5	3.7	3.8	4.5

[a] Simulated for a second-order system with the Bruker package PANIC. [b] Calculated according to refs 54 and 56 using a Boltzmann distribution from the grid search ensemble. [c] Calculated according to refs 54 and 56 from a trajectory ensemble. [d] Back-calculated from experimental values.

have established that the rates of overall and internal motions occur on similar time scales. In the present study computational methods appropriate for the *fast internal motion model* ($\tau_e < \tau_c$) were systematically used to calculate relaxation parameters and spectral densities were expressed with the model-free formalism.[33] It was assumed that overall molecular reorientation and internal motion are not correlated.

Carbon Relaxation Data. In the case of heteronuclear carbon relaxation data, internuclear distances were considered to be fixed, and the spectral densities were as follows:

$$J_n(\omega) = {}^2/_5[S^2(k,l)\tau_c/(1 + (\tau_c\omega)^2) + (1 - S^2(k,l))\tau(k,l)/(1 + (\tau(k,l)\omega)^2)] \quad (6)$$

where $S^2(k,l)$ and $\tau(k,l)$ are the generalized order parameter and effective correlation time of internal motion ($\tau(k,l)^{-1} = \tau_c^{-1} + \tau_e(k,l)^{-1}$), respectively. ω is the frequency of the transition and the indexes k and l refer to the carbon−hydrogen relaxation matrix. The generalized order parameter is defined as follows:

$$S^2(k,l) = 4\pi/5 \sum_{m=-2}^{2} \sum_{i=1}^{N} |Y_{2m}(\theta(k,l),\phi(k,l))/\langle r(k,l)^{-3}\rangle|^2 \quad (7)$$

where $Y_{2m}(\theta(k,l),\phi(k,l))$ are the normalized second-rank spherical harmonics and $\theta(k,l)$ and $\phi(k,l)$ are the polar angles of the internuclear vector taken with respect to the molecular coordinate system.[60] The term $\langle r(k,l)^{-3}\rangle$ represents the carbon−carbon distance matrix averaged in the minus third power. When the angular, S^2_{ang}, and radial contributions the dipole interactions are assumed to be independent, S^2 can be expressed as follows:

$$S^2(k,l) = S^2_{ang}(k,l)\langle r(k,l)^{-3}\rangle^2 \quad (8)$$

In these equations the angular order parameter matrix, $S^2_{ang}(k,l)$, characterizes the amplitudes of the internal motions (for a totally flexible molecule $S^2_{ang}(k,l) = 0$ whereas in the case of a rigid molecule $S^2_{ang}(k,l) = 1$).

When internal motion is extremely rapid ($\tau_e \ll \tau_c$) the second term in (6) is negligible and this simplified expression was used for interpreting relaxation data according to the motional model described by McCain and Markley[13] ($S^2 = 0.89$). In all cases the C−H bond length was considered to be constant at 1.11 Å. No correction was made for the contribution of distant protons (those not directly bonded to the carbon under study) to the relaxation of a given carbon.

Homonuclear Relaxation Data. As regards homonuclear relaxation data, internuclear distances fluctuate and the expressions for the spectral densities become

$$J_n(\omega) = {}^2/_5\{S^2(k,l)\tau_c/(1 + (\tau_c\omega)^2) + (\langle r(k,l)^{-6}\rangle - S^2(k,l))\tau(k,l)/(1 + (\tau(k,l)\omega)^2)\} \quad (9)$$

where $S^2(k,l)$ and $\tau(k,l)$ are defined as above.

Theoretical estimations of $S^2(k,l)$ and $S^2_{ang}(k,l)$ were established from the coordinate sets of the MD simulations. To remove overall translation and rotation, the N trajectory frames were reoriented prior to averaging by a mass-weighted rms fit of the structure to a reference structure which was arbitrarily defined as that of the midpoint frame of the MD simulation.

Theoretical NOESY values were computed with in-house software from ensemble average distance matrixes using the full relaxation matrix method without a correction for leakage due to relaxation mechanisms other than dipole−dipole relaxation. The value of the overall tumbling time was that estimated from the carbon relaxation data and a method previously described[41] was used to establish optimized *experimental* values for the $S^2_{ang}(k,l)$ and $\tau(k,l)$ matrixes. In this approach structural groups (such as methylene moieties or protons belonging to a common ring) were defined and attributed a common value of $S^2_{ang}(k,l)$ and $\tau(k,l)$. Fitting of the theoretical NOESY volume matrix, obtained from back-calculation of the relaxation matrix using eq 9, to the experimental one was achieved by minimizing the squared residue functions. In this procedure the $S^2_{ang}(k,l)$ and $\tau(k,l)$ group values were treated as adjustable parameters.

Finally, theoretical values of NOESY volumes were also calculated with the $S^2_{ang}(k,l)$, $\langle r(k,l)^{-3}\rangle$, and $\langle r(k,l)^{-6}\rangle$ matrixes evaluated from the MD trajectories. In this case, molecular reorientation and internal motion correlation times were those estimated from the carbon relaxation data.

Results and Discussion

Molecular Statics. The potential energy surface (PES) of sucrose in the HGFB force field has previously been described in detail by Tran and Brady.[19] The adiabatic map of sucrose resulting from the grid search is shown in Figure 2 and corresponds closely to the previous one published by Tran and

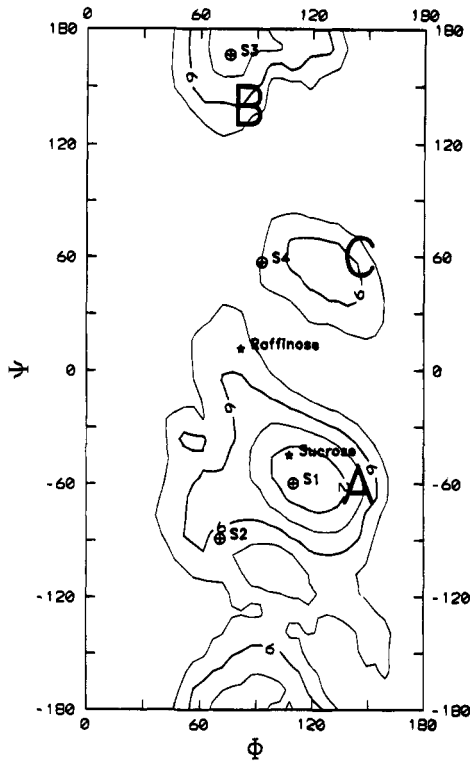

Figure 2. Adiabatic map of sucrose with indications of the positions of the crystallographic conformation of sucrose[1] and of the sucrosyl derivative raffinose.[63] Minima found in MM3[28] are indicated by respectively **S1**, **S2**, **S3**, and **S4**.

Brady.[19] The only significant difference in the map from the previous work is that the local minimum in the C well is found to be 4.2 kcal/mol above the global minimum, in comparison to the 2.7 kcal/mol difference found by Tran and Brady. Bearing in mind that the shape and the location of the C well are practically identical we conclude that this discepancy is caused by different recording techniques and slightly different partial charge allocations. The energetics of the C well in vacuum is sensitive to the local electrostatic environment. The partial charge allocation used in the present work is available as supplementary material.

The adiabatic map contains three major potential energy wells labeled A−C according to Tran and Brady. Its shape can be described as a small belt spanning almost the whole Ψ space, roughly in the region $\Phi = 40-160°$. Two out of the three wells are centered about the eclipsed conformation in Φ, far from ideal exo-anomeric conformation. In contrast, the three wells are centered almost perfectly in idealized staggered positions in the Ψ direction. The crystal structure[1] belongs to the lowest energy well A, indicating that solid state conformational preferences are governed by local steric considerations rather than differences in the hydrogen-bonding network. Within 8 kcal/mol the occupied area in (Φ,Ψ) space is 17% and the calculated 3D volume is 135×10^3 deg^2 kcal/mol; the partition function of the grid search ensemble was about 4.6 at 300 K. These numbers reflect a fairly restricted (Φ,Ψ) space having, for example, about two-thirds of the area and about three-quarters of the volume of a $\beta(1\rightarrow4)$ linked lactoside.[42]

Analysis of the Dynamics Simulations. *Glycosidic Trajectories.* During the combined 1.2 ns simulation in water and 1.0 ns simulation in vacuum we observed only two interwell transitions in (Φ,Ψ) space (see Figure 3d,e). In a simple two-state system, 200 transitions are needed to provide 10% accuracy on the population distribution.[61] Therefore, it is impossible to establish any interwell population distribution from the relatively sparse statistical material available. This statistical problem is inherent in today's state-of-the-art Newtonian molecular dynamics in condensed phases, and the only way to estimate interwell populations is through comparison of properties calculated from trajectories in different wells, with respect to experimental data.

While the extremes of the 1 ns in vacuum trajectory **TSV** (Figure 3a) almost perfectly follow the 6 kcal/mol contour on the adiabatic map, it is obvious that the added water in the **TSX** simulation (Figure 3b) has changed the molecular potential. Although the **TSX** trajectory tends to stay within the 8 kcal/mol contour, it leaves the southern part of the adiabatic A well unexplored and begins to populate the two western (left) wings of the A well.

In agreement with a previous MD study by Tran and Brady[20] and with the shape of the adiabatic potential energy surface, an asymmetrical fluctuation behavior in Φ and Ψ is observed in the vacuum simulation (Table 4). In water, as seen from the glycosidic fluctuations in the **TSX** trajectory, this asymmetry has disappeared. Water is expected to add a frictional damping to the internal motions of the solute, but as can be seen in Table 4, the rms fluctuations in the Φ and Ψ angles in the vacuum simulation (**TSV**) are only between one-half and two-thirds of that of the **TSX** and **TS1** simulations which populate the same well. These observations are in agreement with the study on maltose in solution by Brady and Schmidt,[31] and we believe that this effect can be explained by the changed ("softened") molecular potential. Intramolecular hydrogen bonds are less frequent in solution (Figure 6) which gives the sucrose solute a more extended conformation with slightly more motional freedom. This is indicated by the average value of the radii of gyration in the two simulations (Table 4) which were calculated to 3.22 and 3.27 Å in respectively the vacuum and the solution A-well simulations.

While the calculated trajectories are much too short to establish interwell populations they can give relatively high accuracy for the intrawell population distributions. Figure 7 shows the normalized population distribution of the **TSX** trajectory. The crystal conformation of sucrose[1] is located in the center of the most highly populated area. The fact that the crystal conformation of the sucrose moiety in raffinose[62] also appears in a highly populated area is noteworthy. On the basis of this information it is tempting to suggest that the conformational shift induced by the water is responsible for the creation of the crystal nucleus which is able to propagate in the raffinose case.

Events Correlated to Transitions in (Φ,Ψ) Space. In the trajectory started in the **S2** conformation we observe a slow transition in Ψ (Figure 3d). The trajectory leaves the southwestern wing of the A well between the 59th ps and the 60th ps, to enter the center of the A well in an almost eclipsed Φ position. A slow but steadily increasing value of the Ψ angle starting from 57 ps seems to provoke the concerted motion of the small lateral kink in Φ, the breaking of the O-6g···HO-6f hydrogen bond and the formation of a relatively short-lived glycosidic HO-2g···O-1f hydrogen bond. During the approximately 7 ps that the trajectory stays in the central region of the A well two primary hydroxyl group transitions are observed, an almost abrupt transition in ω_f and a oscillatory transition in ω_g. The still increasing Ψ value followed by a small abrupt variation in the Φ angle leads the trajectory to visit the northwestern region of the A well from where a slow 20 ps transition to the B well with larger than normal oscillations in the Φ and Ψ angles is observed.

In the **TS3** trajectory a large variation in Ψ is observed accompanied by a sharp transition in ω_g at the end of the

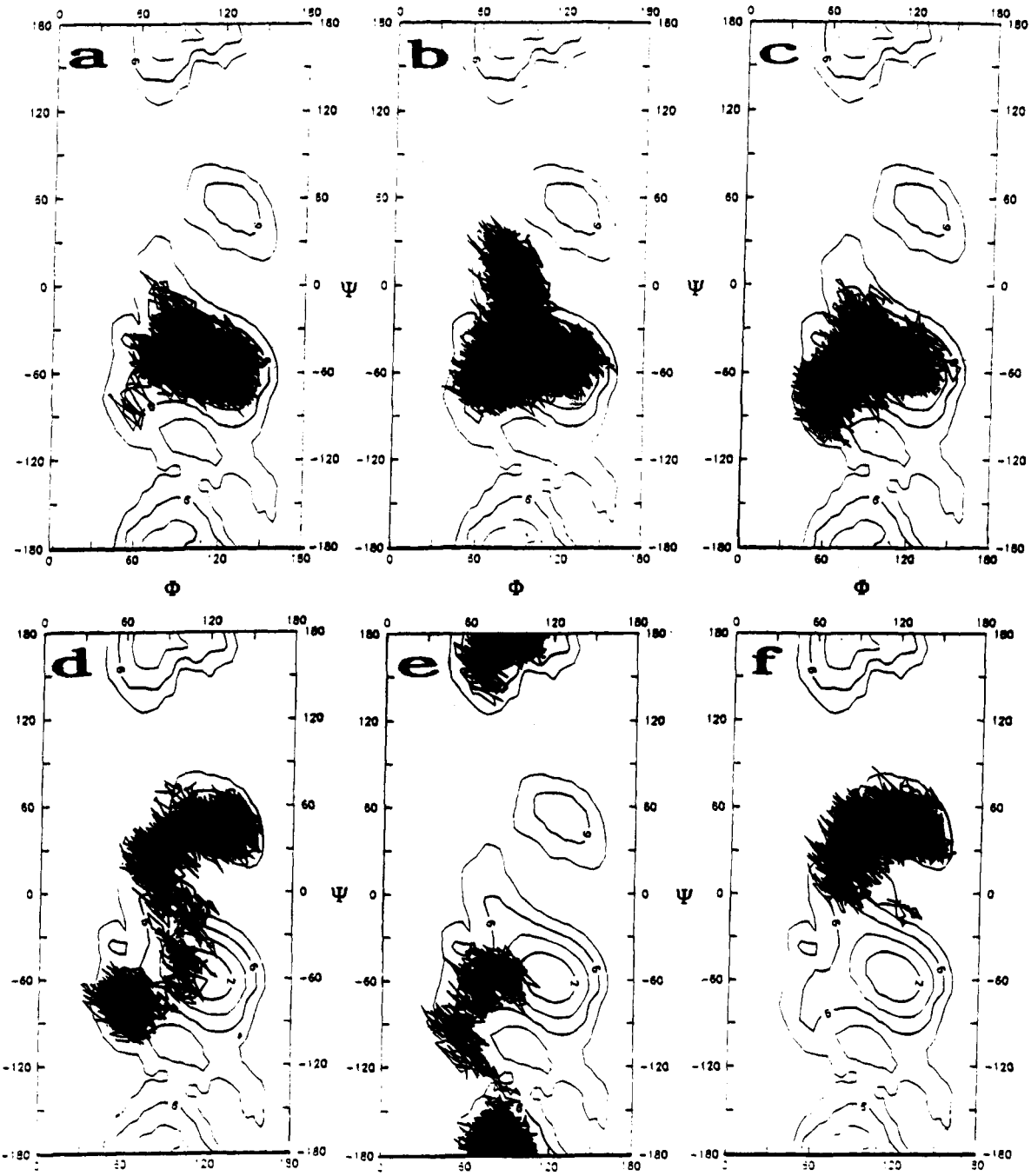

Figure 3. Trajectories of sucrose displayed in dihedral space and superimposed on the adiabatic "in vacuum" map: (a) **TSV**, (b) **TSX**, (c) **TS1**, (d) **TS2**, (e) **TS3**, and (f) **TS4** trajectories.

trajectory. Accordingly, this simulation was prolonged to 170 ps. Indeed, a transition from the C well to the southwestern wing of A well subsequently occurred. In this trajectory the transition pattern seems to be due to the destabilizing effect of the abrupt transition of the ω_g dihedral after 147 ps. No formation or breaking of hydrogen bonds is directly involved in this transition. However, it is likely that the O-2g···HO-3f hydrogen bond destabilizes the molecular potential of the C well. This bond is relatively stable but was broken abruptly at 140 ps. A similar transition was previously reported in a vacuum study by Brady and Tran[20] following the same pathway and one can therefore speculate that the C well will be largely emptied by this low-energy transition pathway to the more favorable A well. It is also possible to argue that a competitive equilibrium exists between the two wells[20] and that this equilibrium is what Christofides and Davies[5] observed in ^{1}H NMR studies of sucrose in DMSO solution where hydrogen bonding to the solvent plays a very minor role. The latter theory is in agreement with the in vacuum competition between the O-2g···HO-1f and O-2g···HO-3f internal hydrogen bonds. In water, internal hydrogen bonds are much less important, and both our simulations here and the experimental data support a one-well system corresponding to the former theory.

Furanosyl Puckering Trajectories. To investigate the influence of the β-D-fructofuranose puckering upon heating and solvation we calculated trajectories in (q_2,ϕ_2) puckering space (see Figure 4). This type of fructosyl puckering investigation is inspired by the early molecular mechanics studies by Warshell and Levitt[63] on ribofuranose. The fructofuranosyl puckering in the MM3 force field[23,24] has previously been described by Pérez et al.[26] It was found that all but one of the 20 observed crystal structures of β-D-fructofuranose, including that of sucrose, belong to a global minimum northern well close to the $^4T_3$ conformation. The adiabatic energy barrier separating the

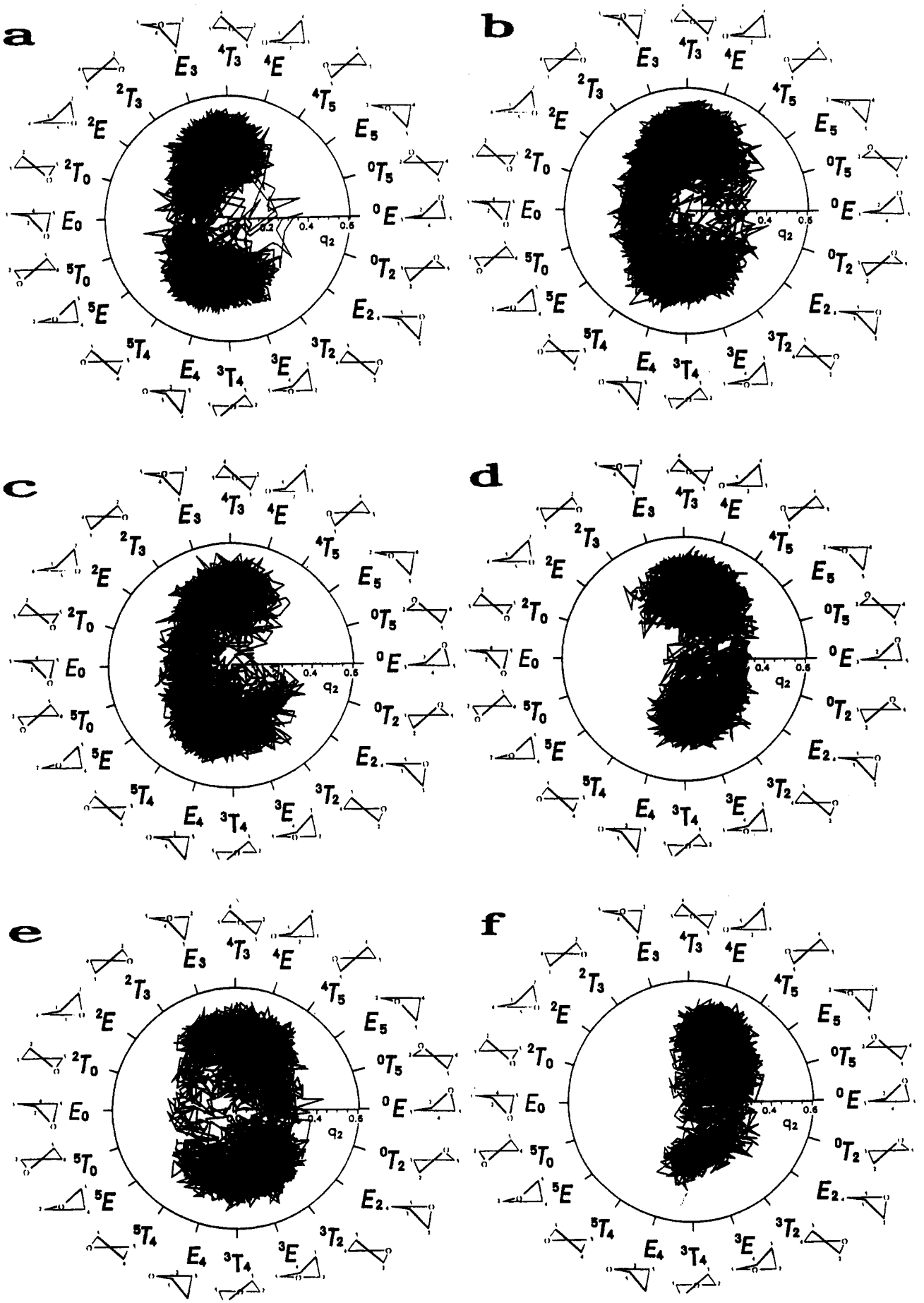

Figure 4. Fructofuranosyl puckering. Trajectories of sucrose displayed in Cremer–Pople puckering space: (a) **TSV**, (b) **TSX**, (c) **TS1**, (d) **TS2**, (e) **TS3**, and (f) **TS4** trajectories.

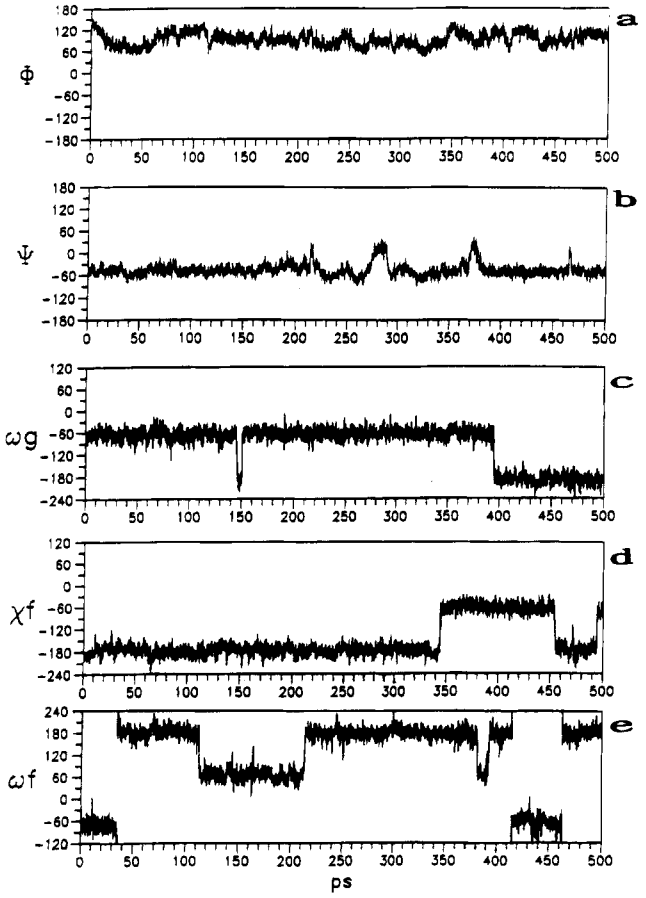

Figure 5. Time series monitoring important dihedral angles from the **TSX** trajectory: (a) Φ, (b) Ψ, (c) ω_g, (d) χ_f, and (e) ω_f.

TABLE 4: Calculated Average Values and Rms Fluctuations of the Φ and Ψ Dihedrals and the Radius of Gyration[a] of Sucrose (Time Intervals in picoseconds, Angles in degrees, and Distances in angstroms)

trajectory[b]	t	⟨Φ⟩	rms fluc Φ	⟨Ψ⟩	rms fluc Ψ	⟨R_g⟩	rms fluc R_g
TSV (A)	100−1000	112.7	12.6	−53.3	9.7	3.22	0.07
TSX (A)	20−500	92.5	18.7	−45.1	18.5	3.27	0.06
TS1 (A)	10−230	85.6	23.4	−57.0	16.1	3.27	0.06
TS2 (AB)	10−150	93.6	29.9	−6.2	56.7	3.30	0.12
TS2 (A)	10−55	61.4	9.0	−75.4	8.2	3.19	0.05
TS2 (B)	70−150	113.5	21.1	40.2	15.5	3.38	0.09
TS3 (C)	10−145	88.8	9.0	−174.7	9.1	3.43	0.06
TS3 (A)	160−170	77.8	11.6	−54.3	8.2	3.22	0.03
TS4 (B)	10−150	100.3	19.0	42.6	13.7	3.29	0.08

[a] Radius of gyration is defined as $R_g^2 = \sum_i m_i r_i^2 / \sum_i m_i$. [b] In parentheses: indications of which potential energy well the trajectory is exploring (see Figure 2).

one crystal conformation belonging to the southern well from those in the northern well was found to be about 2.5 kcal/mol and the eastern pathway (through ^{0}E) was slightly lower in energy than the western pathway (through E_0). The all-planar β-ring transition state was found to be about 1.5 kcal/mol higher than the eastern and western transition states. From these data, which indicate that the energies of puckering transitions are comparable to the formation and breaking of hydrogen bonds, one would expect frequent transitions in the puckering space of the fructofurnosyl ring of sucrose when heated up to 300 K in the MD simulations of sucrose. Our results for trajectories in the A well (Figure 4a−c) are in good qualitative agreement with these findings. In the **TSV**, **TSX**, and **TS1** trajectories we observe that the southern well is populated 30, 50, and 60%, respectively, but due to limitations in the statistical material available we are not able to establish a reliable population distribution (only 25, 12, and 8 transitions are observed respectively). The majority of the transitions belonging to the three A well trajectories travels through the western pathway and only the **TSX** trajectory significantly populates the eastern pathway region. This puckering transition behavior of the MD simulations is somehow surprising since the western pathway is believed to be destabilized in comparison to the eastern pathway due to steric interactions.[17]

The major influence of the solvent with respect to the fructofuranose puckering seems to be a general broadening of the available conformational space, a lowering of the western and eastern barrier potentials and, perhaps, an increase in the population of the southern well. The latter phenomenon can be explained by the fact that the northern conformation of the fructofuranosyl ring, as has also been observed for arabinofuranose,[64] places all the ring hydrogens in axial positions resulting in a small hydrophobic surface pointing towards the solvent. This is also seen in the polarization of the molecule. A single-point evaluation of the MM3 dipole moments in the **S1** conformation results in approximately 5 and 4 D for respectively the northern and the southern well. However, the relatively high population of the southern conformations in the MD simulations is in disagreement with the recent coupling constant study by Duker and Serianni,[17] who proposed that the fructofuranosyl puckering of sucrose in solution is similar to that of the crystalline state ($^4T_3$) with optical rotation investigations suggesting northeastern puckering of the fructofuranosyl moiety of sucrose,[15] and with our analysis of coupling constants and NOESY volumes (vide supra). In the vacuum trajectory, **TSV**, transitions in fructofuranosyl puckering are correlated to transitions in the ω_f dihedral, whereas we find no obvious solute structure correlations with the fructofuranosyl puckering in the condensed phase simulation.

From the trajectories initiated from the **S2**, **S3**, and **S4** conformations (Figure 4d−f) we calculated the relative populations of the southern well to be respectively 40, 65, and 10%. These trajectories seem to prefer the eastern pathway for transitions between the northern and the southern well, especially the **TS2** and the **TS4** trajectories. Both explore the B well and exhibit more restricted puckering behavior. The **TS2** trajectory goes from mainly northern puckering to mainly southern puckering after about 85 ps just after the Ψ transition is completed, and this puckering transition is highly correlated with the formation of a quite persistent interresidue O-5g··HO-3f hydrogen bond. The latter bond may be considered to be the result of this transition rather than its driving force. In the **TS3** trajectory, the fructofuranosyl puckering can be belatedly associated with transitions in ω_g which are in turn related to the Ψ transition. It is conceivable that the puckering transition from south to north at about 128 ps is the real impetus for the transition from the C well to the A well. A similar correlation seems to exist between the puckering in the C well and the occurrence of the relatively persistent intermolecular O-2g··HO-3f hydrogen bond.

Intramolecular Hydrogen Bonding in Water. One of the open questions concerning sucrose solvation is the persistence of intramolecular hydrogen bonds. In the vacuum trajectory two strong hydrogen bonds, O-2g··HO-1f and O5-g··HO-6f, and one weaker hydrogen bond, O-1g··HO-6f are observed, all persisting more than three-quarters of the total time. In the 500 ps solution trajectory (**TSX**) the most populated intramolecular hydrogen bond, O-2g··HO-1f occurs for less than 2% of the time (see Figure 6a). Nevertheless, intramolecular hydrogen bonds are occasionally formed between other hydrogen bonding

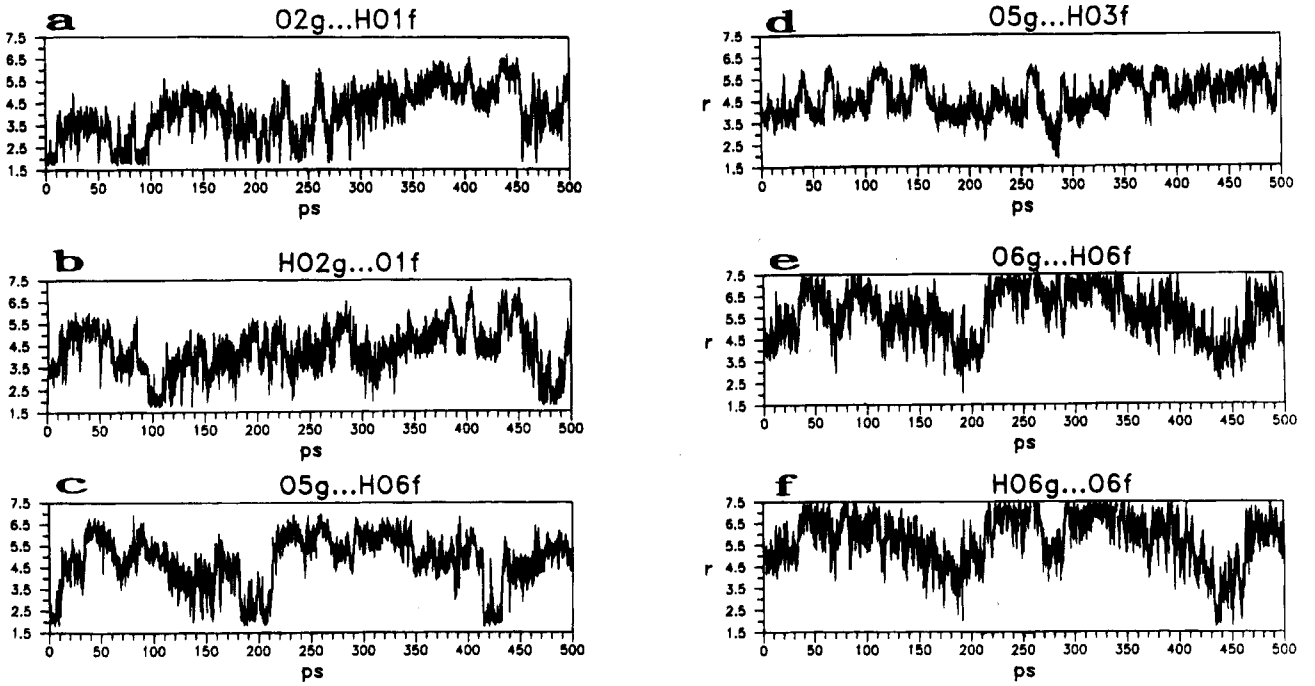

Figure 6. Time series monitoring important hydrogen bonding distances in the **TSX** trajectory: (a) O-2g··HO-1f, (b) HO-2g··O-1f, (c) O-5g··HO-6f, (d) O-5g··HO-3f, (e) O-6g··HO-6f, and (f) HO-6g··O-6f.

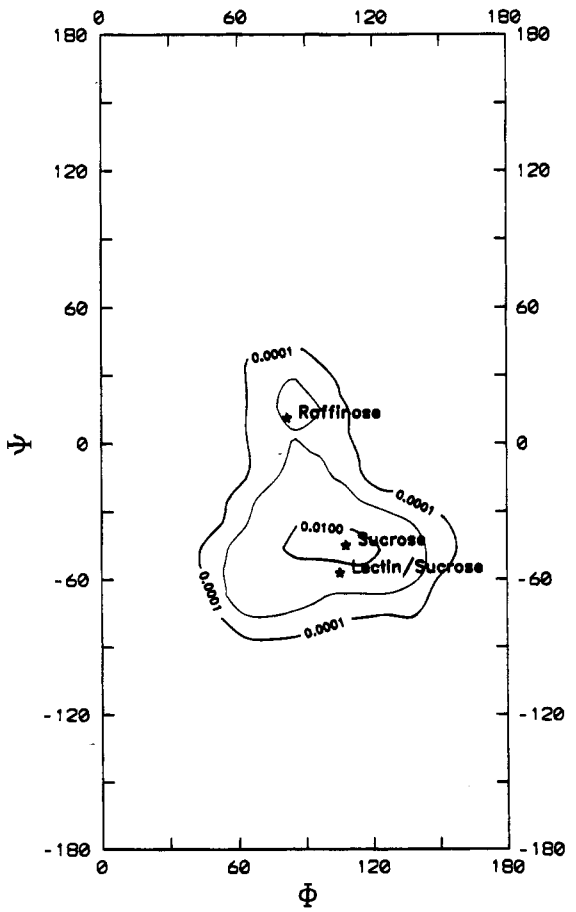

Figure 7. Population density map calculated from the **TSX** trajectory with indication of the crystalline sucrose and raffinose positions.

pairs (O-1g··HO-6f, HO-2g··O-1f, O-5g··HO-3f, O-5g··HO-6f and even between the two primary hydroxyl groups). During the **TSX** trajectory, the average interproton distance between HO-2g and HO-1f was calculated to be 4.3 Å.

In the other A well trajectory, **TS1**, a similar intramolecular hydrogen bonding scheme is observed where only the O-2g··HO-1f one is significantly populated (13%) and some rare events of hydrogen bonding between the primary (C-6) hydroxyl groups occur. In the **TS2** trajectory one almost persistent O-6g··HO-6f hydrogen bond is seen prior to the **TS2** transition. Following this transition, both the high populated HO-2g··O5f interaction and especially the O-5g··HO-3f hydrogen bond seems to stabilize the B well conformations. These observations are consistent with those of the **TS4** trajectory which also explores the B well where the O5g··HO-3f hydrogen bond is highly populated with an average distance of 2.62 Å (rms fluctuation 0.75 Å). During the **TS3** C well trajectory a very different hydrogen bonding scheme appeared. A relatively persistent O-2g··HO-3f hydrogen bond was observed along with a relatively highly populated O-5g··HO-1f hydrogen bond. Exchanging of the O-2g··HO-3f hydrogen bond for the HO-2g··O-3f one tends to destabilize the O5g··HO-1f bond. This is also the case when the O-2g··HO-3f hydrogen bond is abruptly and permanently broken at about 140 ps prior to the Ψ transition at 147 ps.

The absence of competitive internal hydrogen bonds in the two A-well trajectories **TSX** (see Figure 6) and **TS1** is in slight disagreement with earlier NMR studies,[4,13] which indicate the occurrence of a persistent crystallographic O-2g··HO-1f intramolecular hydrogen bond. However, the results are in agreement with both vibrational studies[9-11] which indicate that this bond is broken in dilute aqueous solutions and with a recent crystal structure of sucrose found in a plant lectin complex.[65]

The two sucrose structures found in the protein possesses typical A well conformations ($\Phi \sim 105°$ and $\Psi \sim 57°$) without internal hydrogen bonding, but with a bridging water molecule between O-2g and O-3f. This situation has a statistical significance of 25% in the **TSX** trajectory. Finally, the very low population of the O-2g··HO-1f hydrogen bond is in good agreement with our previous combined NMR and modeling study on sucrose and its 2-deoxy analogue[8] in which we found a striking similarity in the PES and in the NMR data for the two compounds which can be interpreted only by assuming that the role of this hydrogen bond in solution behavior of sucrose is insignificant. In other solution simulations (**TS4**: O-5g··HO-

3f; **TS3**: O-2g··HO-3f; **TS2/A**: O6g··HO-6f; and **TS2/B**: O-5g··HO-3f) more long-lived intramolecular hydrogen bonds occurred but the persistence of these interactions either correspond to a geometrical necessity (**TS4**, **TS3**, **TS2/B**) or to only metastable situations (**TS2/A**).

Primary Hydroxyl Rotamer Populations. In the 1 ns in-vacuum trajectory the primary hydroxyl group on the glucose residue, ω_g, maintains the TG conformation after the equilibration (it was started in the GG position). This result mirrors the population distribution established with the grid searches, a GG:GT:TG ratio of 9:1:90 (see Table 3). In contrast the **TSX** water solution trajectory conserves the crystalline GG conformation for almost 400 ps with only a short excursion to the TG conformation (see Figure 5c). The GT conformation of ω_g is never visited during either of the two long trajectories started from the crystalline conformation. The **TS1** trajectory was started with the ω_g in the GT conformation, but it lasted only throughout the 10 ps corresponding to the equilibration period, whereafter it spontaneously evolved to the GG conformation (less than 2 ps) and then durably to the TG conformation. During the **TS2** trajectory, only one transition in the ω_g dihedral (related to the transition in Ψ) from the initial GT conformation to the TG conformation occurred. In the **TS3** trajectory a similar correlation is observed between the primary hydroxyl rotamer conformation on the glucose residue and the interwell transition in (Φ,Ψ) space. Here the abrupt transition from TG to GT conformation in the ω_g dihedral seems to induce the interwell transition. During the **TS4** trajectory the initial GT conformation of the ω_g dihedral exhibits some large fluctuations but remains unchanged until after 130 ps, whereupon it evolves to the TG conformation. In general, too few transitions between ω_g rotamers are observed to be able to determine the influence of the solvation upon the conformational preference.

The C-5f−C-6f primary hydroxyl group of the fructose residue, ω_f, exhibits a much more flexible character than the corresponding group of the glucose residue. Even in vacuum about 20 transitions of the ω_f dihedral occur with the GG conformation being the most prevalent (81%). This result does not corroborate the GG:GT:TG ratio of 97:0:3 established from the grid searches (see Table 3) which predict an almost exclusive GG conformation. This minor disagreement can be due to insufficient statistical sampling or perhaps to the neglect of the fructofuranose puckering in the grid searches. Throughout the **TSX** trajectory we observe seven transitions (see Figure 5e), with the TG conformation being the most prevalent (64%). During the **TS1** trajectory (only one transition) the TG rotamer is also the most populated (85%). Solvation has a strong influence on the rotational preference of the ω_f primary hydroxyl group and the trajectories in the B and C wells are also characterized by TG conformations which populates about 60% of the total trajectory time in water.

In general the C-2f−C-1f primary hydroxyl group on the fructofuranose ring, χ_f, exhibited very few transitions; the maximum number of transitions observed for a single trajectory is four. In vacuum the conformational preference seems to be largely the trans orientation which is populated 93% of the time, in good agreement with the molecular statics grid searches which determined the population of this conformation to be 99%. The few transitions observed for this primary hydroxyl group make it quasi impossible to estimate the influence of the solvent. However, the fact that two transitions to the GG conformation are observed in the **TSX** trajectory (relative population of 24%) and that one similar transition is observed in the **TS1** trajectory (relative population of 20%) suggests that this conformation is relatively more persistent in water than in vacuum. Steric considerations presumably remain the most important factor for determining the rotamer populations for the χ_f dihedral. In the **TS1**, **TS2**, and **TS3** trajectories no transitions from the stable TG conformation of the χ_f dihedral are observed. The **TS4** trajectory which populates the B well exhibits the opposite pattern; the initial TG conformation evolves shortly after the equilibration period, whereafter it remains in the GG configuration. The GT configuration is never visited for the χ_f dihedral. Finally the conformational behavior about the C-2f−C-1f primary hydroxyl group in these MD trajectories is in qualitative agreement with labeled coupling constant studies by Duker and Serianni,[17] who suggested that the TG rotamers are the least abundant and that GG or a combination of GG and TG rotamers are highly favored.

Radius of Gyration. In comparison with other disaccharides sucrose possesses a fairly spherical structure, far from maximum extension. In all major potential energy wells A, B, and C, the two ring structures of sucrose are positioned almost perpendicular to each other. However, as seen from Table 4, it is possible to distinguish among the three wells on basis of the average value of the radius of gyration, $\langle R_g \rangle$. In the A well we calculate $\langle R_g \rangle$ values between 3.19 and 3.27 Å, in the B well we calculate $\langle R_g \rangle$ values between 3.29 and 3.38 Å, whereas the only number we have in the C well is 3.43 Å. These values are to be compared with the R_g of 3.17 Å for the crystalline structure. The global minimum A well represents the most contracted structures, and the C well represents the most expanded structures. This is most convincingly demonstrated in the time series monitoring the R_g of the **TS3** trajectory; when the transition from the C well to the A well occurs, the $\langle R_g \rangle$ value jumps from 3.43 to 3.22 Å. By considering only the three longest and statistically most reliable trajectories, **TSV**, **TSX**, and **TS1**, carried out in the A well, it appears that the solvent expands the solute structure. This is to be expected if all hydroxyl groups point outward instead of forming internal hydrogen bonds. The expansion of approximately 1.5% between the vacuum and the solvent simulations is less than the approximately 4% expansion found in proteins.[66]

Geometric Autocorrelation Functions. As indicated above, the expected frictional damping exerted by the solvent could not be inferred from the average values of the root-mean-square fluctuations in the Φ and Ψ dihedrals. These average values are a function of the shape of the molecular potential energy well, and this potential changes significantly when changing from vacuum to water. To investigate this further, the normalized autocorrelation function for the dihedral motions[67] was calculated:

$$C_\Phi(t) = \langle \Delta\Phi(t)\, \Delta\Phi(0) \rangle / \langle |\Delta\Phi(0)|^2 \rangle \qquad (10)$$

as has previously been done for maltose by Brady and Schmidt.[31] The calculated time autocorrelation functions for the root-mean-square fluctuations of Φ and Ψ angles are displayed in Figure 8. It is obvious that the inclusion of explicit water solvent leads to a complete frictional damping of the high-frequency motions of the solute. As revealed from the corresponding spectra of Ψ in the time domain (not shown), the high-frequency motions of the solute in vacuum has peaks around 5.75 ps^{-1} corresponding to a periodicity of about 1 ps. Although a similar periodicity is found for the high frequency motions of the Φ angle in vacuum the amplitude was much weaker and coupled with several lower frequency motions presumably arising from the fluctuations in the fructofuranosyl puckering. The frequency peaks about 5.75 ps^{-1} for Φ and Ψ are in the same range as those found for maltose in vacuum[31] using the same force field. In water all the high frequency motions of Φ

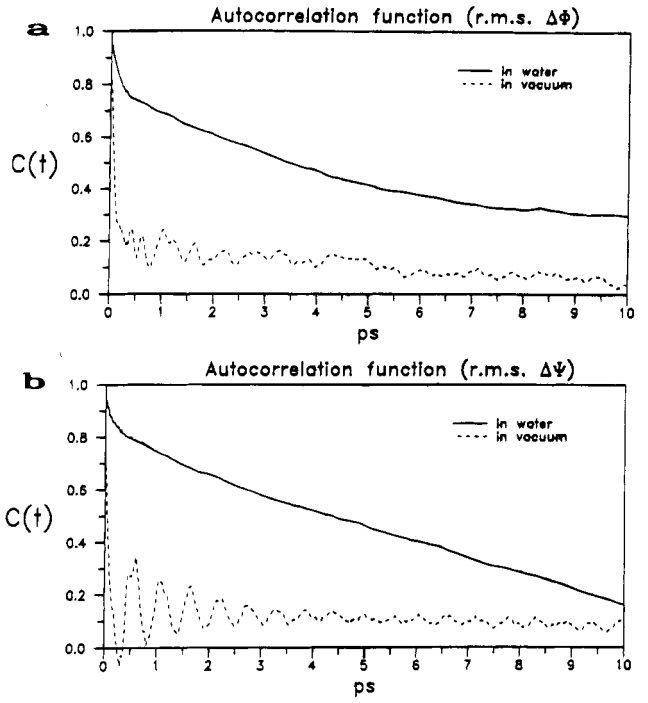

Figure 8. Autocorrelation functions for fluctuations in the glycosidic dihedral angles. Calculated in both vacuum (from the **TSV** trajectory) and in water (from the **TSX** trajectory): (a) Φ and (b) Ψ.

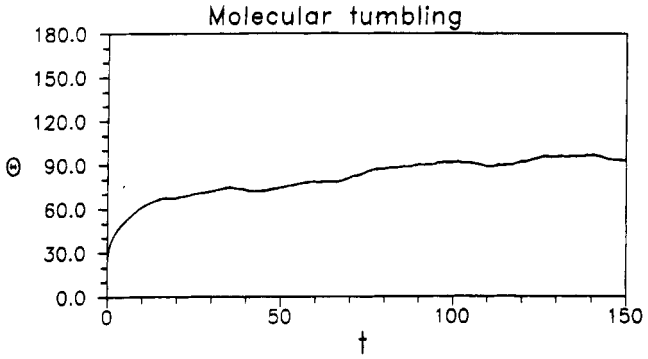

Figure 9. Molecular reorientation. Evolution of the angular diffusion of the solute dipole momentum as calculated from the **TSX** trajectory.

and Ψ are removed and the spectral density for frequencies above 0.3 ps^{-1} corresponding to periodicities of less than 20 ps was negligible. With the sampling rates used in the simulations, we could not investigate frequencies higher than 25 ps^{-1} corresponding to the Nyquist frequency; however, such high frequencies are not believed to be relevant to molecular relaxation.

To establish the overall molecular tumbling time for the solute the angular evolution of the solute dipole moment as expressed by the autocorrelation function for the angular displacement of the dipole moment vector:[29]

$$C_\theta(\Delta t) = \langle \theta_d(t + \Delta t) \rangle \qquad (11)$$

where θ_d is the angle between the dipole vectors at the time t and at the time $t + \Delta t$, and the averaging is performed over the whole trajectory. The result shown in Figure 9 indicates that the angular information is uncorrelated after approximate 110–140 ps. This is in good agreement with the experimental value of 120 ps,[8] corresponding to the NMR correlation time τ_c. The deviations of the asymptotic behavior toward $\theta_d = 90°$ (corresponding to a completely randomized situation) can be explained by the lack of statistical significance especially with respect to fructofuranosyl puckering.

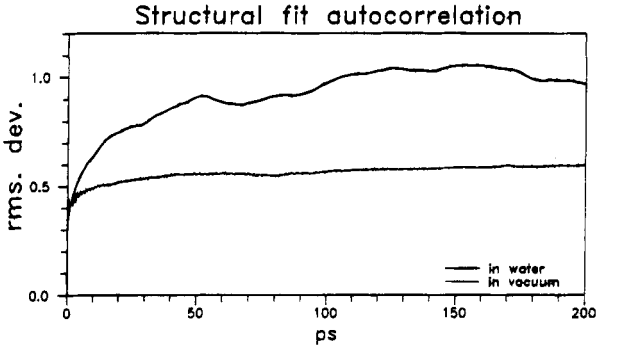

Figure 10. Internal motion relaxation as calculated from structural fit autocorrelation functions.

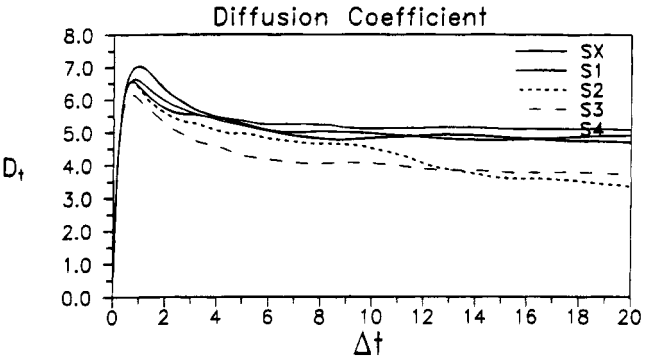

Figure 11. Time series monitoring the center of mass mean square displacement autocorrelation function of the sucrose solute (1/6t). The diffusion coefficient is indicated in 10^{-6} cm^2/s.

To analyze the overall molecular relaxation of the internal motions of the solute, we calculated the structural rms deviation[68] autocorrelation function:

$$C_S(\Delta t) = \langle SF_M(t + \Delta t) \rangle \qquad (12)$$

where SF_M is the mass weighted structural rms fit, and the averaging is done for Δt going from 0 to the length of the trajectory (∞). The resulting function is shown in Figure 10. It was observed that the molecular relaxation calculated for the vacuum trajectory is largely finished after about 0.3 ps. After this period we observe a weak oscillatory behavior about a equilibrium value corresponding to the periodicities as found in the vacuum dihedral autocorrelation functions. In the water environment we observe similar fast molecular relaxation, but in this case the structural decay continues to grow until about 110–140 ps. This relaxation time corresponds to that of reorientation correlation time of the dipole vector and suggests that the molecular relaxation of the internal motions and the molecular tumbling falls within the same time range for sucrose in water.

Self-Diffusion of the Sucrose Solute. The self-diffusion of the solute was calculated by monitoring the Stokes–Einstein relation which becomes valid at long times. Figure 11 shows the diffusion coefficient as a function of the time for the five condensed-phase simulations. The plots have a characteristic peak at about 1 ps, indicating the backscattering maximum after the initial period of free movement. From the plots a diffusion coefficient of 4.9 ± 0.3 × 10^{-6} D in the asymptotic region, in good agreement with experimental determinations is obtained. The diffusion coefficient of sucrose in water solutions can be extrapolated from the Schlieren method measurements by Schliephake[69] to be about 5.1 × 10^{-6} D for a 3–4 w/w % solution at 300 K, it is listed to be 5.21 × 10^{-6} D for a 0.38 w/w % solution at 298 K in the *Handbook of Chemistry and*

Physics[52] and it has been measured by Uedaira and Uedaira[70] using Rayleigh interference method to be 5.23×10^{-6} D at infinite solution and 298 K. Note that the diffusion coefficient decreases with increasing concentration. In contrast to a similar calculation for maltose,[31] which resulted in a calculated diffusion coefficient a factor of 2 lower than the experimental value and which was explained by the less viscous than real TIP3P water, the agreement for sucrose is very good. Previous experience from MD simulations has shown that the asymptotic region is reached in a time much shorter than that required to diffuse a molecular diameter.[71] In agreement with observations made by van Eijck and Kroon,[30] it is observed that (with our sampling frequency) the trajectories of 150 ps constitute the absolute lower limit to give statistically stable estimates of the diffusion coefficient. It is therefore probable that the calculated trajectories for maltose were too short to provide a precise estimation of the diffusion coefficient. However, it cannot be excluded that the relatively extended conformations of maltose as opposed to the more globular conformations of sucrose are important in this type of calculations. In this context, it is interesting to note that the diffusion coefficient for the **TS3** trajectory (see Figure 11), which represents the most extended type of conformation, is underestimated by approximately 20%.

Coupling Constants. Experimental and calculated coupling constants for sucrose have been collected in Table 3. The glucose vicinal ring couplings are in relatively good agreement with experiment which is consistent with the preservation of the $^4C_1$ chair conformation of the glucose residue throughout the simulation. The MD results generally are in better accordance with experiment than the MS results and the inclusion of water has no significant influence upon the glucose ring conformation. In contrast, the calculated fructofuranosyl ring couplings $^3J_{\text{H-3f-H-4f}}$ and $^3J_{\text{H-4f-H-5f}}$ from the MD trajectory are in poor agreement with the experimental values. Indeed, the calculated furanoid ring coupling constants indicate a much better agreement with experimental values when the fructofuranose is conserved in the northern conformation as shown by the calculated couplings from the MS search and from the **TS4** trajectory which mainly explores the northern region (Table 3). This finding is corroborated by the magnitudes of the $^3J_{\text{C-1f,C-5f}}$, $^3J_{\text{C-2f,H5f}}$, and $^3J_{\text{C-3f,C-6f}}$ values of sucrose as compared to those of methyl β-D-fructofuranoside which also indicate a predominate northern population.[17] Before drawing strong conclusions from this apparent discrepancy, it should be recalled that the Haasnoot–Altona equation has not included furanoid systems in the parametrization as the conformational pseudorotational flexibility and the more flat type of furanoid ring conformations makes the additivity constants strongly dependent on the actual torsional angle.[72] When comparing the calculated furanoid coupling constants from the **TSV** and **TSX** trajectories, it is observed that the southern puckering population is further enhanced in the water phase as can be expected by the slightly less hydrophobic character of the fructofuranose ring. Since no experimental data indicate a significant southern population, we must conclude that the HGFB force field does not model properly the fructofuranosyl puckering either in vacuum or in aqueous solution. An analogous underestimation of the northern populations has also been observed for the arabinobiose five-membered rings.[73]

As can be expected from the abnormal rotamer population of the primary glycosyl hydroxyl group, the calculated *pro-R* and *pro-S* coupling constants are in poor agreement with the experimental ones. The very low transition rate of this primary hydroxyl group (only seven transitions are observed throughout the complete 1.2 ns condensed-phase ensemble) makes it obvious that an equilibrium in this respect has not been achieved in any of the simulations. Because of this statistical weakness, it is not possible to assess the influence of solvation upon this equilibrium. However since five of the seven transitions leads to the "forbidden" TG conformation it appears that the erroneous vacuum properties of the force field are dominating the solvation equilibrium.

TABLE 5: Experimental T_1 Values for the Methine (Average for All Ring Positions) and Methylene Carbons of Sucrose

	62.9 MHz 293 K		100.6 MHz			
			293 K	296 K	296 K	296 K
carbons	run 1	run 2	run 3	run 4	run 5	run 6
Glc*p* CH	0.513	0.517	0.478	0.489	0.526	0.504
Fru*f* CH	0.484	0.475	0.449	0.471	0.501	0.478
CH_2-6g	0.288	0.282	0.260	0.284	0.311	0.298
CH_2-1f	0.278	0.292	0.256	0.282	0.282	0.285
CH_2-6f	0.328	0.296	0.298	0.315	0.327	0.316

As regards the β-fructofuranosyl H-6fR and H-6fS protons, it should be pointed out that stereospecific assignments have not been obtained either in the present work or in previous studies even in the case of ^{13}C single-site labeling.[17] The statistical basis for the corresponding C-5f–C-6f primary hydroxyl group transition rate is somewhat better (25 transitions occurred during the complete 1.2 ns condensed phase ensemble) than that of the glucose exo-cyclic group. The calculated *pro-S* coupling constants from the MD trajectories are in good agreement with experiment provided that the assignments be correct and significantly better than that of the vacuum simulations (**MS** and **TSV**), indicating a significant influence of the solvation upon this equilibrium. The *pro-R* couplings calculated from the condensed-phase simulations are high in contrast to those established for the vacuum simulations, which are low. However, it is obvious that the almost exclusive conformational preference GG in vacuum is changed considerably in solution, notably including a dominant TG population. By analogy with structurally related compounds the GG population can be experimentally estimated[17] to be between 20 and 40%, wherefore it appears that this rotamer population is overestimated in the MD trajectories.

The ensemble averaged glycosidic heteronuclear coupling $^3J_{\text{H-1g,C-2f}}$ from the solution trajectories are in good agreement with the experimentally measured 4.2 Hz value. The longest and most statistically significant trajectory **TSX** results in a calculated coupling constant of 4.1 Hz, within the experimental error (Table 3). The good agreement contrasts with the population-averaged value derived from the grid searches and the **TSV** trajectory both performed in vacuum and both being dominated by the influence of the O-2g···HO-1f internal hydrogen bond.

Sucrose NMR Relaxation in Water. *Carbon Relaxation Data.* Six sets of T_1 values, which were established for a 0.06 M aqueous solution of sucrose at 62.9 and 100.6 MHz, are collected in Table 5. Only averaged values for the methine carbons have been given, and temperature fluctuations, which can be roughly estimated at $\pm 2-3$ K, are considered to be largely responsible for variations in experimental values (5–10%). A much more extensive set of carbon relaxation data has been reported by McCain and Markley,[12,13] including a compilation of the influence of magnetic field, temperature, and concentration on these data. Two reproducible aspects of the parameters in Table 5 should be noted. The fructofuranose (Fru*f*) ring carbon T_1 values are consistently lower than those of the glucopyranose (Glc*p*) ring by about 5–7% and the order for the methylene carbon T_1 values is C-1f < C-6g < C-6f with

TABLE 6: Theoretical Carbon Angular Order Parameters, S^2_{ang}, from Dynamics Trajectories of Sucrose

	C-1g	C-2g	C-3g	C-4g	C-5g	⟨Cg⟩	C-3f	C-4f	C-5f	⟨Cf⟩
TS1	0.66	0.69	0.68	0.68	0.69	0.68	0.56	0.30	0.47	0.44
TS2	0.25	0.38	0.38	0.39	0.40	0.36	0.20	0.13	0.42	0.25
TS3	0.75	0.74	0.72	0.72	0.73	0.73	0.57	0.46	0.59	0.54
TS4	0.66	0.71	0.70	0.70	0.72	0.70	0.67	0.54	0.62	0.61
TSX	0.70	0.70	0.69	0.68	0.69	0.69	0.48	0.25	0.51	0.41
TSV	0.75	0.74	0.72	0.72	0.73	0.73	0.46	0.36	0.63	0.47

the exception of run 2. Both of these tendencies were observed in earlier work on 0.5 M aqueous sucrose,[4] whereas almost identical average values were observed for the Glc*p* and Fru*f* rings in a 7/3 mixture of D_2O and DMSO-d_6 at several magnetic fields.[38]

In order to calculate theoretical carbon T_1 values from the MD trajectories, angular order parameters were extracted from these simulations as outlined in the Methods section and these data have been collected in Table 6. With the exception of the **TS2** trajectory which contained a glycosidic transition, the glycosyl ring carbon S^2_{ang} values were close to 0.7, whereas those of the fructofuranosyl ring carbon S^2_{ang} values were between 0.4 and 0.6. The glycosyl S^2_{ang} values were fairly homogeneous, while those of the five-membered ring (particularly C-4f) showed much more scatter both with respect to the ring positions and with respect to the various trajectories. All the values deviated strongly with respect to the average methine carbon order parameter of 0.89 established by McCain and Markley[13] based on more than 400 carbon relaxation measurements. In their fitting of experimental relaxation data with the model-free formalism,[33] these authors considered that internal motion was extremely fast with respect to molecular reorientation and they neglected the second term in eq 1. This approximation has been widely adopted in carbon relaxation studies of carbohydrates.[39,40]

From analysis of the autocorrelation function for the condensed-phase simulations we suspected that very rapid internal motion would not be relevant for the calculation of NMR relaxation data of sucrose and that internal motion was best described by a correlation time closer to 0.1 ns (vide supra). Moreover, simulations of homonuclear relaxation data also suggested that internal motion was occurring *on the same time scale* as that of molecular reorientation (vide infra). Accordingly, carbon T_1 values were plotted as a function of overall tumbling for both motional models (solid curve for all carbons with $S^2_{ang} = 0.89$ and $\tau \ll \tau_c$; dashed curve for the Fru*f* ring carbons with $S^2_{ang} = 0.65$ and $\tau = 0.5\ \tau_c$ and dotted curve for the Glc*p* ring carbons with $S^2_{ang} = 0.75$ and $\tau = 0.3\ \tau_c$) at 62.9 and 100.6 MHz (Figures 12 and 13, respectively). Margins of experimental error (vertical bars) have also been indicated. It can be seen from these plots that both motional models correctly reproduce the experimental carbon T_1 data over a wide range of correlation times (see inserts). This range of τ_c values should cover the experimental data previously reported.[12,13] Indeed, considerable variations in the viscosity (and thus τ_c) of sucrose solutions were observed as a result of changes in either concentration or temperature.

Extensive simulations of experimental heteronuclear Overhauser effects described earlier[13,18] were not conducted as no data was available for dilute (<0.1 M) aqueous solution. However, it was verified that the results obtained for 1 M sucrose at 300 K ($\tau_c = 0.357$ ns) could be reproduced with the MD motional model upon fine-tuning of the τ_c values (~1–1.1 τ_c).

It should be pointed out that it is not likely that molecular reorientation and internal motion have identical energy barriers,

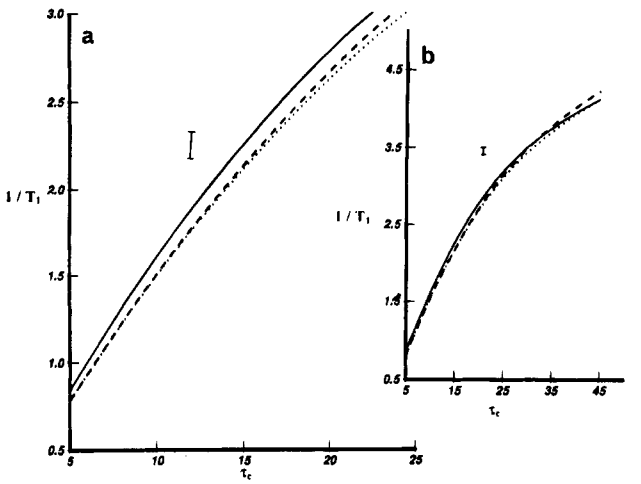

Figure 12. Plot of $1/T$ as a function of molecular reorientation, τ_c, for methine carbons at 100.6 MHz. (a) Solid line for the McCain and Markley[13] motional model, $S^2_{ang} = 0.89$; dashed line for fructofuranosyl, $S^2_{ang} = 0.65$, $\tau = 0.5\ \tau_c$ and dotted line for the glucopyranosyl $S^2_{ang} = 0.75$ and $\tau = 0.3\ \tau_c$. (b) Solid line as in (a); dashed line for fructofyranosyl, $S^2_{ang} = 0.65$, $\tau = 0.4\ \tau_c$ and dotted line for the glucopyranosyl $S^2_{ang} = 0.75$ and $\tau = 0.2\ \tau_c$.

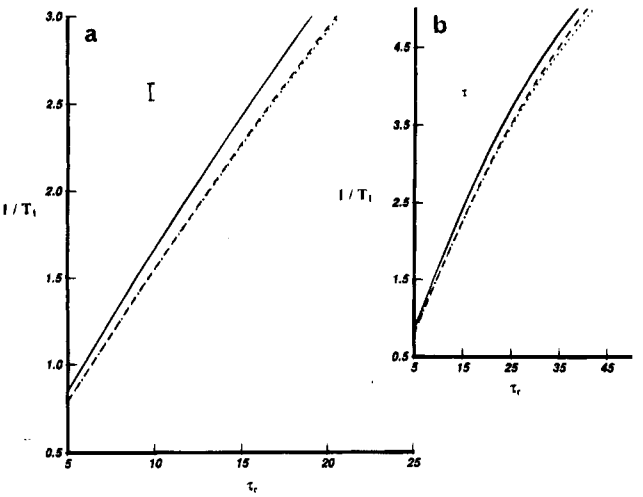

Figure 13. Plot of $1/T$ as a function of molecular reorientation, τ_c, for methine carbons at 62.9 MHz. Key as in Figure 12.

and therefore relative rates of motion would be expected to vary with the temperature (and thus τ_c). For example, it has been shown from carbon relaxation studies that the gap between τ and τ_c increases at lower temperatures for methyl group rotation in a disaccharide. Decreasing the τ/τ_c ratio to 0.4 and 0.2 for the internal motion for the Fru*f* and Glc*p* rings, respectively, leads to only a moderate increase in the gap in the plots for the two motional models (Figure 12b).

Thus, it would appear that the temperature dependence of the carbon longitudinal relaxation times are not significantly different for the two motional models under consideration. Moreover, the magnetic field dependence of the carbon T_1 data for the two motional models are very similar, and it was not possible to discriminate between them on this basis either. Accordingly, the τ_c value of 0.14 ns, which is in agreement with the motional model extracted from the MD simulations (Glc*p*: $\tau_e = 0.06$ ns; Glc*p*/Fru*f*: $\tau_e = 0.06$ ns; Fru*f*: $\tau_e = 0.14$ ns), has been used for simulations of homonuclear relaxation parameters.

Proton Relaxation Data. The proton angular order parameters for the various MD trajectories are given in Table 7. Again,

TABLE 7: Theoretical Proton Angular Order Parameters, S^2_{ang}, from Dynamics Trajectories of Sucrose (Average Values for the Various Spins)

	Glc*p* ring	Glc*p*/ CH_2-6g	H-1g/ CH_2-1f	Glc*p*/ Fru*f*	CH_2-6g	CH_2-6g/ Fru*f*	CH_2-1f	Fru*f*/CH_2-1f, CH_2-6f	Fru*f* ring	CH_2-6f
TS1	0.69	0.65	0.32	0.69	0.61	0.64	0.40	0.47	0.52	0.18
TS2	0.37	0.36	0.32	0.57	0.28	0.54	0.61	0.29	0.21	0.16
TS3	0.76	0.73	0.76	0.76	0.61	0.75	0.71	0.62	0.64	0.19
TS4	0.70	0.62	0.74	0.72	0.34	0.72	0.57	0.58	0.61	0.25
TSX	0.71	0.61	0.47	0.71	0.41	0.64	0.36	0.50	0.51	0.13
TSV	0.76	0.75	0.68	0.75	0.63	0.74	0.56	0.64	0.55	0.45

TABLE 8: Experimental (Standard Deviation)[a] and Theoretical[b] NOESY Volume Matrixes of Sucrose at 400.13 MHz

	H-1g	H-2g	H-4g	H-1f (CH_2)	H-3f	H-4f	H-6fg (CH_2) + H-5fg + H-3g
H-1g	**0.462 (0.012)**	**−0.054 (0.001)**		**−0.035 (0.004)**	**−0.004 (0.001)**	**−0.006 (0.003)**	**−0.007 (0.001)**
TS1	0.504	−0.058		−0.032	−0.001	0.000	−0.010
TS3	0.573	−0.063		−0.005	−0.040	0.000	−0.008
TS4	0.506	−0.060		−0.001	−0.002	−0.041	−0.022
TSX	0.496	−0.057		−0.035	−0.001	−0.001	−0.010
H-2g		**0.555 (0.024)**	**−0.055 (0.006)**				**−0.029 (0.019)**
TS1		0.574	−0.046				−0.017
TS3		0.572	−0.043				−0.019
TS4		0.570	−0.045				−0.016
TSX		0.575	−0.048				−0.018
H-4g			**0.622 (0.008)**				**−0.055 (0.010)**
TS1			0.580				−0.050
TS3			0.574				−0.052
TS4			0.578				−0.056
TSX			0.651				−0.040
H-1f (CH_2)				**0.111 (0.000)**	**−0.020 (0.003)**		**−0.009 (0.005)**
TS1				0.069	−0.023		−0.004
TS3				0.058	−0.011		−0.025
TS4				0.077	−0.020		−0.005
TSX				0.084	−0.023		−0.005
H-3f					**0.631 (0.010)**	**−0.008 (0.005)**	**−0.042 (0.003)**
TS1					0.697	−0.029	−0.012
TS3					0.644	−0.030	−0.007
TS4					0.670	−0.018	−0.031
TSX					0.694	−0.023	−0.019
H-4f						**0.496 (0.004)**	**−0.062 (0.008)**
TS1						0.635	−0.055
TS3						0.660	−0.047
TS4						0.575	−0.041
TSX						0.647	−0.055
H-6fg (CH_2) H-5fg + H-3g							**0.317 (0.004)**
TS1							0.283
TS3							0.274
TS4							0.300
TSX							0.280

[a] Acquired with a 1 s mixing time at 296 K with a 0.06 M sample. The standard deviation for cross-peak volumes is calculated with four values (average deviation for two values for the diagonal volumes). [b] Key: **TS1**, **TS3**, **TS4**, and **TSX** values are given below the experimental ones (boldface) and standard deviations (in parentheses) in this order. All theoretical values were calculated with the motional model from the ^{13}C data: $\tau_c = 0.14$ ns, $\tau_e = 0.06$ ns with the exception of the intracyclic furanosyl ones ($\tau_c = 0.14$ ns).

the relative amplitude of the internal motion of the pyranosyl ring is more reduced ($0.69 < S^2_{ang} < 0.75$) than for the furanosyl moiety ($0.51 < S^2_{ang} < 0.64$). The values of S^2_{ang} are similar for all the simulations with the exception of **TS2** which is characterized by much lower values reflecting the occurrence of an interwell transition. As these values are not compatible with the physical motional model established from the ^{13}C relaxation data, this trajectory has been ignored in the calculations of NOESY volumes from the geometric data of the MD simulations.

The homonuclear S^2_{ang} values for the methylene protons mirror the corresponding carbon data with relative average (**TS1**, **TS2**, **TS3**, **TS4**, and **TSX**) amplitudes of 0.49, 0.51, and 0.14 for CH_2-6g, CH_2-1f, and CH_2-6f, respectively. The exocyclic group S^2_{ang} values are strongly correlated with the number of transitions amongst the staggered rotamer conformations. However, as the vicinal proton coupling constants are not correctly reproduced by the MD trajectories, it is not clear how relevant these parameters are with respect to simulations of NOESY volumes.

The theoretical 250.13 and 400.13 MHz NOESY volume matrixes were established with the MD motional model for all the trajectories. In previous work,[28] it was shown that a very poor fit is obtained for theoretical values with the *rigid molecule approximation* (in particular, the H-1g diagonal volume is far too weak, 0.345 at 400.13 MHz). Normalized NOESY volumes acquired at 400.13 MHz and 250.13 MHz with a mixing time of 1 s have been collected in Tables 8 and 9, respectively, along with the theoretical values for the **TS1**, **TS3**, **TS4**, and **TSX** trajectories. A correction has not been applied to account for relaxation due to mechanisms other than dipolar interactions and therefore theoretical values should be slightly higher (5−10%) than experimental ones.

Very different interactions between H-1g and the fructofura-

TABLE 9: Experimental (Standard Deviation)[a] and Theoretical[b] NOESY Volume Matrixes of Sucrose at 250.13 MHz

	H-1g	H-2g H-4g	H-1f (CH_2)	H-3f	H-4f	H-6fg (CH_2) + H-5fg + H-3g
H-1g	**0.436 (0.033)**	−0.074 (0.008)	−0.039 (0.006)	−0.008 (0.003)	−0.007 (0.001)	−0.021 (0.003)
TS1	0.469	−0.068	−0.031	−0.001	−0.001	−0.011
TS3	0.533	−0.075	−0.004	−0.048	0.000	−0.009
TS4	0.467	−0.070	−0.001	−0.002	−0.046	−0.024
TSX	0.459	−0.068	−0.035	0.001	−0.001	−0.011
H-2g + H-4g		**0.564 (0.044)**	−0.004 (0.002)	−0.006 (0.005)		
TS1		0.484	0.001	0.00		
TS3		0.481	0.000	0.002		
TS4		0.482	0.000	0.000		
TSX		0.518	0.001	0.000		
H-1f (CH_2)			**0.069 (0.003)**	−0.019 (0.008)		
TS1			0.054	−0.024		
TS3			0.036	−0.012		
TS4			0.051	−0.021		
TSX			0.062	−0.025		
H-3f				**0.589 (0.052)**	−0.006 (0.004)	−0.056 (0.012)
TS1				0.671	−0.034	−0.014
TS3				0.609	−0.035	−0.008
TS4				0.637	−0.021	−0.037
TSX				0.667	−0.027	−0.022
H-4f					**0.432 (0.011)**	−0.082 (0.020)
TS1					0.608	−0.061
TS3					0.630	−0.052
TS4					0.543	−0.044
TSX					0.621	−0.063

[a] Acquired with a 1 s mixing time at 296 K with a 0.06 M sample. The standard deviation for crosspeak volumes is calculated with four values (average deviation for two values for the diagonal volumes). [b] Key: **TS1**, **TS3**, **TS4**, and **TSX** values are given below the experimental ones (boldface) and standard deviations (in parentheses) in this order. All theoretical values were calculated with the motional model from the ^{13}C data: $\tau_c = 0.14$ ns, $\tau_e = 0.06$ ns with the exception of the intracyclic furanosyl ones ($\tau_c = 0.14$ ns).

nosyl protons were predicted for the various MD trajectories: either with the CH_2-1f moiety (a cross-peak volume of roughly −0.035, **TS1** and **TSX**), or with H-3f (−0.040, **TS3**), or with H-4f (−0.041, **TS4**). Detection of experimental interring cross-peak volumes at 400.13 MHz between H-1g and CH_2-1f (−0.035), H-1g and H-3f (−0.004), and H-1g and H-4f (−0.006) suggested that the **TSX** (**TS1**) conformers are the major species and that small but significant (5−10%) populations of **TS3** and/or **TS4** structures are also present.

From inspection of the intraring furanosyl cross-peak volumes from the **TS4** trajectory, which is the only one with a predominate population of northern puckering families, it is possible to evaluate the puckering preferences of the five-membered ring. The H-3f/H-4f (−0.018) and H-3f/H-5f (−0.031) theoretical volumes decrease and increase, respectively, with respect to the corresponding **TSX** and **TS1** volumes (**TSX**, −0.023 and −0.019; **TS1**, −0.029 and −0.012) in better agreement with the experimental values (−0.008 and −0.042). The H-4f diagonal volume (0.575 for an experimental value of 0.496) is much improved, indicating that globally the summed cross-relaxation rates are reasonable. However, this is partially due to the interglycosidic interaction with H-1g (−0.041) which represents a minor population. Concomitantly, the H-4f/(H-5g + CH_2-6f) volume is much too weak (−0.041 for −0.062) as a result of the interglycosidic and exocyclic group orientations, respectively. This latter volume would be expected to be much higher for more favorable values of Φ, Ψ, and ω_f (cf. −0.055 for **TS1** and **TSX**). It can be concluded that, as was the case for the coupling constant data, NOESY volumes are best represented by the northern puckering families.

Analysis of the methylene proton volumes is very difficult due to both strong coupling effects and internal rotation which both lead to enhanced volumes. Indeed, the experimental diagonal volumes of the methylene protons are expected to be roughly 150% of the theoretical values for first order systems owing to strong coupling effects.[74] As provision for these latter effects has not been made in the NOESY volume calculations, the corresponding volumes in Table 8 are very reasonable.

A predominant GG population for the glucosyl exocyclic groups is only observed for the **TSX** trajectory (Table 3), but the fit for H-4g/CH_2-6g volume is poorer (−0.040 for −0.055). The **TS4** simulation which gives the best fit for the H-5g/CH_2-6g coupling constants also affords to best agreement for the H-4g/CH_2-6g cross-peak volume (−0.056 for −0.055) corroborating a major GT population for this hydroxylmethyl group. As stated previously, an important H-4f/CH_2-6f cross-relaxation rate is indicated by the experimental NOESY volumes associated with H-4f suggesting that the predominant rotameric form for the CH_2-6f moiety is TG in keeping with the major rotamer evidenced by the vicinal coupling constant data.

In this section it has been seen that a similar description of the conformational preferences for the glycosidic linkage and the two pendant groups at the six positions is obtained from either homonuclear coupling constants or NOESY volumes. The motional model established from the carbon relaxation data is very satisfactory for calculating the NOESY volumes. Further fine-tuning of the motional model would improve the fit with respect to the experimental data. However, until a better representation of the furanosyl ring-puckering and pendant group populations is available, such efforts would seem premature.

The most important aspect of this work has been to establish a motional model which is consistent with both proton and carbon relaxation data. From the autocorrelation function of the dynamics trajectories, it appeared that high-frequency oscillations of sucrose were severely damped by the presence of explicit water and that internal motions on the same time scale as overall tumbling were occurring. This corroborates previous work on carbohydrates, where it has been shown that relaxation data was modulated by motion with correlation times near 0.1 ns. Even in the case of Me β-Gal*p*,[75] all the intracyclic interactions were influenced by analogous slow motion. Moreover, generally speaking heuristic exploration of internal

dynamics of small carbohydrates either affords a unique motional model of the type reported here ($\tau_e \sim 0.1$ ns; sucrose[28] and Me β-Gal$p$[75]) or both a model analogous to the one established in this work ($\tau_e = 0.1$ ns) as well as a model consistent with the aforementioned studies[12,13] ($\tau \ll \tau_c$, sucralose[41] and ethyl β-lactoside[42,75]). Although this latter model reproduces the experimental NOESY volumes almost as well, it is totally incompatible with the amplitudes of internal motions which are evaluated from the MD trajectories.

The slow motion ($\tau_e \sim 0.1$ ns) which is modulating the NMR relaxation parameters can best be described as puckering relaxation of the sugar rings. In our hands, vacuum trajectories of disaccharides lead to S^2_{ang} values in the range 0.7−0.8 for pyranosyl rings and 0.4−0.5 for furanosyl rings, while corresponding S^2_{ang} values of a polyaromatic molecule like anthracene are very near 1. In contrast the large-amplitude glycosidic transitions must be much slower. Indeed, it has been shown[41] that if interwell glycosidic transitions were occurring on a time scale similar to that of τ_c, the interproton $S^2_{ang}(k,l)$ values would be much lower as is the case with **TS2**. Furthermore, few such transitions were observed during the total nanosecond of the condensed-phase trajectories.

Conclusions

It has been the aim of the present work to establish, through joint molecular modeling and high-resolution data, the structural and dynamical features of sucrose in dilute aqueous solution. From extensive molecular dynamics simulation with explicit water molecules, it has been shown that the low energy region of Φ,Ψ space is significantly shifted and somewhat enlarged with respect to the calculation in vacuum. As a result, the predominant solution conformation encompasses the crystal conformation of sucrose, as well as that of the sucrosyl raffinose. Nevertheless, other conformational wells are represented, being only moderately less accessible that the main region. Very few interwells interconversions have been observed in the course of the dynamics simulation in water. The sucrose molecule is found to be extensively bound to water molecules. On average, around 25 water molecules constitute the first hydration shell.[76] Clearly, all the potential intramolecular hydrogen bonds are exchanged to these surrounding water molecules. It is to be noted that a water bridging conformation O-2g···Ow···O-3f persists durably (25%) and of the two crystalline intramolecular hydrogen bonds (O-2g···HO-1f and O-5g···HO-6f) neither exhibits a significant lifetime in aqueous solution. Coupled with the observation that the primary hydroxyl group also exhibits conformational transitions, it must be concluded that the conformational features of crystalline sucrose do not survive once the molecule is solvated. This conclusion is corroborated by the good agreement between theoretical and experimental transport coefficients such as the translational diffusion coefficients and the molecular reorientational time.

An important aspect of the work has been to establish a motional model which is consistent both with the high resolution NMR relaxation data and with the molecular dynamics simulation. In particular, a unified description of both proton and carbon relaxation has been reached. In our motional description of sucrose, we have found that the internal motions occur on a time scale comparable to that of the overall tumbling. The similarity in time scales for overall and internal motions have led us to evaluate the full dipolar interaction, both angular and distance contributions, from the molecular dynamics trajectories. In contrast, the large-amplitude glycosidic transitions must be much slower as it has been shown[41] that if the interwell glycosidic transitions were occurring on a time scale similar to τ_c, the interproton $S^2_{ang}(k,l)$ values would be much lower. Molecular dynamics simulations would have to be extended into the microsecond range to accurately encompass the structures and conformations that could influence time-averaged experimental data. In the event that the internal dynamics described by these MD simulations correctly represent the conformational behavior of aqueous sucrose, it would appear that the reduced model-free spectral densities are not appropriate for small carbohydrates.

Acknowledgment. This work was supported by a grant to S.B.E. in the framework of the program Conception Macro-Molecules Assistée par Ordinateur (Organibio). The provision of financial support by P. et M. Curie University, CNRS (URA 1679), and INRA are acknowledged. The authors would like to express their appreciation to Professor J. W. Brady and Dr. R. K. Schmidt (Cornell University) for being helpful with the implementation of the carbohydrate force field in the QUANTA/CHARMm package, and S.B.E. wants to thank Professor J. W. Brady in particular for inspiring and knowledgeable tutoring in the domain of condensed-phase MD simulations. Last but not least Dr. R. Loris (Vrije Universitet Brussel, Belgium) is thanked for access to Lectin/sucrose coordinates prior to publication.

Supporting Information Available: Table of atomic charges for the sucrose solute (1 page). Ordering information is given on any current masthead page.

References and Notes

(1) Brown, G. M.; Levy, H. A. *Acta Crystallogr. Sect. B.* **1973**, *29*, 790−797.
(2) Hanson, J. C; Sieker, L. C.; Jensen, L. H. *Acta Crystallogr. Sect. B.* **1973**, *29*, 797−808.
(3) Pérez, S. In *Sucrose. Properties and Applications*; Mathlouthi, M., Reiser, P., Eds.; Blackie Academic and Professional: London, 1995; pp 11−30.
(4) Bock, K.; Lemieux, R. U. *Carbohydr. Res.* **1982**, *100*, 63−74.
(5) Christofides, J. C.; Davies, D. B. *J. Chem. Soc., Chem. Commun.* **1985**, 1533−1534.
(6) Davies, D. B.; Christofides, J. C. *Carbohydr. Res.* **1987**, *163*, 269−274.
(7) Adams, B.; Lerner, L. *J. Am. Chem. Soc.* **1992**, *114*, 4827−4829.
(8) Hervé du Penhoat, C.; Imberty, A.; Roques, N.; Michon, V.; Mentech, J.; Descotes, G.; Pérez, S. *J. Am. Chem. Soc.* **1991**, *113*, 3720−3727.
(9) Mathlouthi, M.; Luu, D. V. *Carbohydr. Res.* **1980**, *81*, 203−212.
(10) Mathlouthi, M.; Luu, C.; Meffroy-Biget, A. M.; Luu, D. V. *Carbohydr. Res.* **1980**, *81*, 213−223.
(11) Mathlouthi, M. *Carbohydr. Res.* **1981**, *91*, 113−123.
(12) McCain, D. C.; Markley, J. L. *Carbohydr. Res.* **1986**, *152*, 73−80.
(13) McCain, D. C.; Markley, J. L. *J. Am. Chem. Soc.* **1986**, *108*, 4259−4264.
(14) Mulloy, B.; Freinkel, T. A.; Davies, D. B. *Carbohydr. Res.* **1988**, *184*, 39−46.
(15) Stevens, E. S.; Duda, C. A. *J. Am. Chem. Soc.* **1991**, *113*, 8622−8627.
(16) Poppe, L.; van Halbeek, H. *J. Am. Chem. Soc.* **1992**, *114*, 1092−1094.
(17) Duker, J. M.; Serianni, A. S. *Carbohydr. Res.* **1993**, *249*, 281−303.
(18) Girlich, D.; Lüdemann, Z. *Naturforsch.* **1993**, *48c*, 407−413.
(19) Tran, V. H.; Brady, J. W. *Biopolymers* **1990**, *29*, 961−976.
(20) Tran, V. H.; Brady, J. W. *Biopolymers* **1990**, *29*, 977−997.
(21) Brooks, B.; Bruccoleri, R.; Olafson, B.; States, D.; Swaminathan, S.; Karplus, M. *J. Comput. Chem.* **1983**, *4*, 187−217.
(22) Ha, S. N.; Giammona, A.; Field, M.; Brady, J. W. *Carbohydr. Res.* **1988**, *180*, 207−221.
(23) Allinger, N. L.; Yuh, Y. H.; Lii, J.-H. *J. Am. Chem. Soc.* **1989**, *111*, 8551−8567.
(24) Allinger, N. L.; Rahman, M.; Lii, J.-H. *J. Am. Chem. Soc.* **1990**, *112*, 8293−8307.
(25) French, A. D.; Dowd, M. K. *J. Mol. Struct. (THEOCHEM)* **1993**, *286*, 183−201.
(26) Pérez, S.; Meyer, C.; Imberty, A.; French, A. In *Sweet-taste Chemoreception*; Mathlouthi, M., Kanters, J. A., Birch, G. B., Eds.; Elsevier: 1993; pp 55−73.

(27) Lichtenthaler, F. W.; Immel, S.; Martin, D.; Müller, V. *Starch/Stärke* **1992**, *44*, 445−456.
(28) Casset, F.; Imberty, A.; Hervé du Penhoat, C.; Koca, J.; Pérez, S., submitted.
(29) Brady, J. W. *J. Am. Chem. Soc.* **1989**, *111*, 5155−5165.
(30) van Eijck, B. P.; Kroon, J. *J. Mol. Struct.* **1989**, *195*, 133−146.
(31) Brady, J. W.; Schmidt, R. K. *J. Phys. Chem.* **1993**, *97*, 958−966.
(32) Brady, J. W. *Curr. Opinion Struct. Biol.* **1991**, *1*, 711−715.
(33) Lipari, G.; Szabo, A. *J. Am. Chem. Soc.* **1982**, *104*, 4546−4559.
(34) Homans, S. W.; Forster, M. *Glycobiology* **1992**, *2*, 143−51.
(35) Hricovini, M.; Shah, R. N.; Carver, J. P. *Biochemistry* **1992**, *31*, 10018−10023.
(36) Meyer, C.; Pérez, S.; Hervé du Penhoat, C.; Michon, V. *J. Am. Chem. Soc.* **1993**, *115*, 10300−10310.
(37) McCain, D. C.; Markley, J. L. *J. Magn. Reson.* **1987**, *73*, 244−251.
(38) Kovacs, H.; Bagley, S.; Kowalewski, J. *J. Magn. Reson.* **1989**, *85*, 530−541.
(39) Bagley, S.; Kovacs, H.; Kowalewski, J.; Widmalm, G. *Magn. Reson. Chem.* **1992**, *30*, 733−739.
(40) Kowalewski, J.; Widmalm, G. *J. Phys. Chem.* **1994**, *98*, 28−34.
(41) Bouchemal-Chibani, N.; Braccini, I.; Derouet, C.; Hervé du Penhoat, C.; Michon, V. *Int. J. Biol. Macromol.*, in press.
(42) Engelsen, S. B.; Pérez, S.; Braccini, I.; Herve du Penhoat, C. *J. Comput. Chem.*, in press.
(43) IUPAC-IUB, Commission on Biochemical Nomenclature, *Arch. Biochem. Biophys.* **1971**, *145*, 405−421.
(44) Altona, C.; Sundaraligam, M. *J. Am. Chem. Soc.* **1972**, *94*, 8205−8212.
(45) Cremer, D.; Pople, J. A. *J. Am. Chem. Soc.* **1975**, *97*, 1354−1358.
(46) Macura, S.; Huang, Y.; Suter, D.; Ernest, R. R. *J. Magn. Reson.* **1981**, *43*, 259−281.
(47) Neuhaus, D.; Williamson, M. In *The Nuclear Overhauser Effect in Structural and Conformational Analysis*; VCH Publishers: New York, 1989; p 292.
(48) Jorgensen, W. L. *J. Am. Chem. Soc.* **1981**, *103*, 335−340.
(49) Verlet, L. *Phys. Rev.* **1967**, *159*, 98−103.
(50) van Gunsteren, W. F.; Berendsen, H. J. C. *Mol. Phys.* **1977**, *34*, 1311−1327.
(51) Engelsen, S. B.; Brady, J. W.; Sherbon, J. W. *J. Agric. Food Chem.* **1994**, *42*, 2099−2107.
(52) *Handbook of Chemistry and Physics*, 64th ed.; Weast, R. C., Ed.; CRC Press: Cleveland, 1983−1984; F-46, D-266.
(53) Allen, M. P.; Tildesley, D. J. *Computer Simulations of Liquids*; Clarendon Press: Oxford, 1991; p 60.
(54) Haasnoot, C. A. G.; de Leeuw, F. A. A. M.; Altona, C. *Tetrahedron* **1980**, *36*, 2783−2792.
(55) Moore, W. J. In *Physical Chemistry*; Longman Harlow: Essex, UK, 1972.
(56) Tvaroska, I.; Hricovini, M.; Petrakova, E. *Carbohydr. Res.* **1989**, *189*, 359−362.
(57) Bock, K.; Duus, J. Ø. *J. Carbohydr. Chem.* **1994**, *13*, 513−543.
(58) Werbelow, L. G.; Grant, D. M. *Adv. Magn. Reson.* **1977**, *9*, 189−299.
(59) Carver, J. P. *Curr. Opinion Struct. Biol.* **1991**, *1*, 716−720.
(60) Tropp, J. *J. Chem. Phys.* **1980**, *72*, 6035−6043.
(61) Pastor, R. W. In *Proteins: Structure, Dynamics and Design*; Renugopalakrishnan, V., Carey, P. R., Smith, I. C. P., Huang, S. G., Storer, A. C., Eds.; ESCOM: Leiden, 1991; p 229−233.
(62) Berman, H. M. *Acta Crystallogr. Sect. B* **1970**, *26*, 290−299.
(63) Warshel, A.; Levitt, M. *J. Am. Chem. Soc.* **1978**, *100*, 2607−2613.
(64) Cros, S.; Hervé du Penhoat, C.; Pérez, S.; Imberty, A. *Carbohydr. Res.* **1993**, *248*, 81−93.
(65) Loris, R., private comunications.
(66) van Gunsteren, W. F.; Karplus, M. *Biochemistry* **1982**, *21*, 2259.
(67) Brooks III, C. K.; Karplus, M.; Pettitt, B. M. *Proteins: A Theoretical Perspective of Dynamics, Structure and Thermodynamics*; Advances in Chemical Physics, LXXI; Wiley: New York, 1988, and references therein.
(68) Kabsch, W. *Acta Crystallogr. Sect. A* **1976**, *32*, 922−923.
(69) Schliephake, D. *Zucker* **1965**, 138−142.
(70) Uedaira, H.; Uedaira, H. *J. Solut. Chem.* **1985**, *14*, 27−34 and references therein.
(71) Rossky, P. J.; Karplus, M. *J. Am. Chem. Soc.* **1979**, *101*, 1913−1936.
(72) Altona, C.; Haasnoot, C. A. *Org. Magn. Reson.* **1980**, *13*, 417−429.
(73) Cros, S; Imberty, A.; Bouchemal, N.; Hervé du Penhoat, C.; Pérez, S. *Biopolymers* **1994**, *34*, 1433−1447.
(74) Keeler, J.; Neuhaus, D.; Williamson, M. P. *J. Magn. Reson.* **1987**, *73*, 45.
(75) Engelsen, S. B.; Koca, J.; Braccini, I.; Herve du Penhoat, C.; Pérez, S. *Carbohydr. Res.*, in press.
(76) Engelsen, S. B.; Pérez, S., unpublished data.

JP950424T